EXPERIMENTS WITH A 5-LEVEL GLOBAL PRIMITIVE EQUATION ATMOSPHERIC MODEL USING ANALYTICALLY DETERMINED FIELDS

Dennis Edward Maher

NAVAL POSTGRADUATE SCHOOL
Monterey, California

THESIS

EXPERIMENTS WITH A 5-LEVEL GLOBAL
PRIMITIVE EQUATION ATMOSPHERIC MODEL
USING ANALYTICALLY DETERMINED FIELDS

by

Dennis Edward Maher

September 1974

Thesis Advisor: R. T. Williams

Approved for public release; distribution unlimited.

SECURITY CLASSIFICATION OF THIS PAGE (When Data Entered)

REPORT DOCUMENTATION PAGE		READ INSTRUCTIONS BEFORE COMPLETING FORM
1. REPORT NUMBER	2. GOVT ACCESSION NO.	3. RECIPIENT'S CATALOG NUMBER
4. TITLE (and Subtitle) Experiments with a 5-Level Global Primitive Equation Model Using Analytically Determined Fields		5. TYPE OF REPORT & PERIOD COVERED Master's Thesis September 1974 6. PERFORMING ORG. REPORT NUMBER
7. AUTHOR(s) Dennis Edward Maher		8. CONTRACT OR GRANT NUMBER(s)
9. PERFORMING ORGANIZATION NAME AND ADDRESS Naval Postgraduate School Monterey, California 93940		10. PROGRAM ELEMENT, PROJECT, TASK AREA & WORK UNIT NUMBERS
11. CONTROLLING OFFICE NAME AND ADDRESS Naval Postgraduate School Monterey, California 93940		12. REPORT DATE September 1974 13. NUMBER OF PAGES 93
14. MONITORING AGENCY NAME & ADDRESS(if different from Controlling Office) Naval Postgraduate School Monterey, California 93940		15. SECURITY CLASS. (of this report) Unclassified 15a. DECLASSIFICATION/DOWNGRADING SCHEDULE

16. DISTRIBUTION STATEMENT (of this Report)

Approved for public release; distribution unlimited.

17. DISTRIBUTION STATEMENT (of the abstract entered in Block 20, if different from Report)

18. SUPPLEMENTARY NOTES

19. KEY WORDS (Continue on reverse side if necessary and identify by block number)

Global atmospheric model
Analytic initial data
Second order differencing
Fourth order differencing
Cross-polar flow

20. ABSTRACT (Continue on reverse side if necessary and identify by block number)

A description of the FNWC five level baroclinic, global, primitive equation model is presented including the finite difference equations used. Analytic initial data is generated in order to avoid the complications caused by real data with respect to verification. A comparison of second order differencing versus mixed second and fourth order differencing shows that the latter gives relatively more accurate propagation for smaller scale disturbances than the former. In addition various experiments are conducted to improve the model's

DD FORM 1 JAN 73 1473 EDITION OF 1 NOV 65 IS OBSOLETE
S/N 0102-014-6601 |
(Page 1)

SECURITY CLASSIFICATION OF THIS PAGE (When Data Entered)

treatment of cross-polar flow.

Experiments with a 5-Level Global Primitive Equation Atmospheric Model Using Analytically Determined Fields

by

Dennis Edward Maher
Lieutenant, United States Navy
B.B.A., University of Toledo, 1968

Submitted in partial fulfillment of the
requirements for the degree of

MASTER OF SCIENCE IN METEOROLOGY

from the

NAVAL POSTGRADUATE SCHOOL
September 1974

ABSTRACT

A description of the FNWC five level baroclinic, global, primitive equation model is presented including the finite difference equations used. Analytic initial data is generated in order to avoid the complications caused by real data with respect to verification. A comparison of second order differencing versus mixed second and fourth order differencing shows that the latter gives relatively more accurate propagation for smaller scale disturbances than the former. In addition various experiments are conducted to improve the model's treatment of cross-polar flow.

TABLE OF CONTENTS

LIST OF CHARTS

LIST OF FIGURES

LIST OF SYMBOLS AND ABBREVIATIONS

A	Arbitrary amplitude constant in A^*
A^*	Arbitrary constant in stream function
a	Earth's radius
B	Arbitrary constant in stream function
c_o	phase speed of fastest gravity wave
c_p	specific heat for dry air at constant pressure
D	5° grid distance at equator
D_u	Lateral diffusion of latitudinal momentum
D_v	Lateral diffusion of longitudinal momentum
D_T	Lateral diffusion of heat
D_q	Lateral diffusion of specific humidity
D_m	Lateral diffusion of momentum
FNWC	Fleet Numerical Weather Central
F_u	Frictional stress (latitudinal direction)
F_v	Frictional stress (longitudinal direction)
f	Coriolis parameter
g	Acceleration of gravity
H	Diabatic heating
i	Longitudinal grid index
$\vec{i}$	Unit longitudinal vector
j	Latitudinal grid index
$\vec{j}$	Unit latitudinal vector
k	Vertical grid index

m	Wave number
mb	Millibars
NACA	National Advisory Committee on Aeronautics
N	Wave number plus one - m + 1
n	Time step superscript
P	Pressure
Q	Moisture source/sink term
q	Specific humidity
R	Specific gas constant for dry air
S	Stability coefficient
T	Temperature
t	Time
u	Zonal wind
v	Meridional wind
w	Measure of vertical velocity, positive upward $w = -\dot{\sigma} = -\frac{d\sigma}{dt}$
z	Height
Δt	Time increment
Δx	Distance increment in the x-direction - $a \Delta\lambda \cos\theta$
α	Specific volume
θ	Latitude
$\Delta\theta$	Distance increment in the latitudinal direction
λ	Longitude
$\Delta\lambda$	Distance increment in the longitudinal direction
ν	Angular wave velocity
π	Terrain pressure

$\Delta\pi$	Change in terrain pressure
σ	Dimensionless vertical coordinate, $0 \leq \sigma \leq 1$, increasing downward
$\Delta\sigma$	Layer thickness (vertical distance increment)
$\dot{\sigma}$	Measure of vertical velocity - $\frac{d\sigma}{dt}$, -w
ϕ	Geopotential
$\Delta\phi_p$	Change in geopotential on pressure surface
$\Delta\phi_\sigma$	Change in geopotential on sigma surface
ψ	Stream function
∇	Del operator (horizontal)
∇^2	Laplacian operation (horizontal)
*	Supersrcipt indicating first stage of Matsuno time step
< >	Vertical summation of layer contributions of quantity in brackets

ACKNOWLEDGEMENTS

The author wishes to thank Dr. R. T. Williams for his helpful advice, patient guidance and many stimulating ideas. Much appreciation is extended to Dr. G. J. Haltiner for his advice in preparing the final draft of this thesis and for his course in Numerical Weather Prediction which inspired the author to undertake this project. Lt. W. F. Mihok, USN was extremely helpful in supplying copies of the Fortran deck of the model and aided the author many times during this project. Many thanks are extended to the staff of the W. R. Church Computer Center of the Naval Postgraduate School for their enthusiastic support of this work.

I. INTRODUCTION

After the FNWC Northern Hemispheric Primitive-Equation Model became operational (Kesel and Winninghoff, 1972), Dr. F. J. Winninghoff, a former Naval Postgraduate School faculty member, designed and programmed a five-level global primitive equation model utilizing a spherical, staggered grid and the sigma coordinate system. This global atmospheric model was basically a conversion of the operational hemispheric model to a global model using a staggered latitude-longitude grid instead of a polar stereographic projection.

The advantage of a global model is that it treats the entire atmosphere as a physical system. It is reasonable to expect that when the model is fully operational, increased accuracy and range of prediction will result. A global atmospheric model allows tropical circulation to develop freely without artificial boundary conditions. This is crucial since the tropics are the main source region of the energy, which drives the general circulation of the atmosphere. Interactions between the hemispheres are also represented.

The operational use of a global atmospheric model for short range prediction is practical since advanced computers capable of integrating a global model in a reasonable amount of time are presently available and since satellites in the near future are expected to provide more accurate world wide data input.

From a tactical standpoint an operational global atmospheric model is a tremendous advantage since it provides a timely forecast of the

weather anywhere in the world. Improved predictability in the tropics would greatly benefit the Navy since a large percentage of its bases are located in the tropics and many naval operations take place in tropical waters. The most recent example of this is the establishment of U. S. Naval presence in the Indian Ocean and the building of a naval base on Diego Garcia Island in that area.

Elias (1973) modified and carried out further experiments with the Winninghoff global model on the 6500CDC computer located at FNWC. He generated geopotential fields by inserting an analytic spherical harmonic stream function (Neamtan, 1946) into the linear balance equation and solving for the geopotential by successive over-relaxation. The geopotential fields were generated on a 63 x 63 polar stereographic grid and were interpolated onto a 5° Northern Hemisphere latitude-longitude grid after insertion into the global model. Once this interpolation had taken place the fields were reflected into the Southern Hemisphere. Real data analyzed by FNWC objective schemes were also inserted into the global model on a polar stereographic grid and then interpolated onto a spherical grid and reflected into the Southern Hemisphere. In the cases where analytic data were generated, artificial moisture and temperature fields were also produced. The purpose of using an analytic geopotential field instead of real data is that it allows wave number, phase speed and wave amplitude to be specified.

The geopotential fields were used in the linear balance equation to obtain the stream function which provided initial rotational winds. In the analytic cases Elias also avoided numerical balancing by using an analytic solution for the wind fields. His forecasts using analytically

derived winds were well behaved but those using winds from the linear balance equation excited spurious inertial-gravity waves which were undesirable for operational forecasts.

Mihok (1974) and McCollough (1974) converted the FNWC global atmospheric model to operate on the IBM 360 computer at the Naval Postgraduate School. McCollough examined various schemes of initialization of the model using real data from the FNWC objective analyses used by Elias. He found that the use of the Robert (1965) time frequency filter and dynamic balancing using forward and backward averages about the initial value was effective in reducing inertial-gravity wave "noise."

McCollough (1974) pointed out that the method of data input by interpolating to latitude-longitude grid points and to sigma surfaces from a polar stereographic grid on p-surfaces probably introduces some imbalance between mass and wind fields. In order to avoid the problems associated with initializing with real data this study employs a simplified direct analytic solution to the non-linear balance equation (Phillips, 1959). This solution is based on the same spherical harmonic stream function (Haurwitz, 1940, Neamtan, 1946) used by Elias (1973).

McCollough also noted that large gradients developed near the pole when real data were used. This thesis examines the polar problem with an analytic initial state which gives flow over the pole.

Mihok (1974) modified the horizontal spatial difference equations to form a mixed second and fourth order scheme with the aim of improving the phase speeds of the meteorological waves, as proposed by Williams

(1972). He generated analytic fields using the same method as Elias (1974) and also used the same real data as Elias (1973) and McCollough (1974). Mihok derived his winds from the stream function computed by numerically solving the nonlinear balance equation with geostrophic winds used in the Jacobian. The use of this method of balancing introduced inertial-gravity waves which made it difficult to compare the relative merits of forecasts made with the second and fourth order scheme. The experiments in this thesis avoid the balancing problem by employing analytic height and wind fields. Mihok's mixed scheme is compared with the second order scheme for various wave numbers.

II. BAROCLINIC PRIMITIVE EQUATION MODEL

The five-level global atmospheric primitive equation model currently under development by FNWC and the Naval Postgraduate School is used in this study. The primitive equations are written in spherical coordinates with sigma used vertically. They are similar to the equations used by Smagorinsky et al (1965), Arakawa et al (1969) and Kesel and Winninghoff (1972). Finite differencing of these equations takes place on a grid staggered both horizontally and vertically.

The finite difference form of the primitive equations contain Arakawa's (1966) technique for conserving energy. Fictitious kinetic energy is not produced by the integration of the nonlinear advective terms. However, difference form of the hydrostatic equation used in the model does not meet the restrictions placed on differencing in the vertical if total energy is to be conserved. A discussion of the requirements for total energy conservation may be found in Haltiner (1971). The difference equation used in the model is similar to the one used by Kesel and Winninghoff (1972). They state that the reason for differencing the hydrostatic equation in this manner is to reconcile the initial temperature, height and surface pressure analyses with the forecast variables in the model.

A complete list of the finite difference equations, similar to the list given by Mihok (1974), is provided in Appendix A. The fourth order modifications to the difference equations (Mihok, 1974) are stated in Appendix B.

The heating and moisture source terms, lateral diffusion terms and frictional stress terms are not included in Appendix A but are the same as those used in the operational FNWC Northern Hemispheric Primitive-Equation Model (Kesel and Winninghoff, 1972). For the purpose of this study the heating and moisture source terms and lateral diffusion terms are turned off.

A flat earth (all terrain heights at sea level) is used in this study since it was desirable to avoid the instability experienced by McCollough (1974) when terrain height was included.

A. PRIMITIVE EQUATIONS

The continuous form of the equations used in the model are as follows:

Longitudinal momentum equation

$$\frac{\partial(u\pi)}{\partial t} = -\frac{1}{a\cos\theta}\left[\frac{\partial uu\pi}{\partial\lambda} + \frac{\partial(uv\pi\cos\theta)}{\partial\theta}\right] + \frac{\pi\partial(wu)}{\partial\sigma} + \frac{\pi uv\tan\theta}{a} + \pi vf - \frac{1}{a\cos\theta}\left[\frac{\pi\partial\theta}{\partial\lambda} + RT\frac{\partial\pi}{\partial\lambda}\right] + \pi F_u + D_u \qquad (1)$$

Latitudinal momentum equation

$$\frac{\partial(v\pi)}{\partial t} = -\frac{1}{a\cos\theta}\left[\frac{\partial(uv\pi)}{\partial\lambda} + \frac{\partial(vv\pi\cos\theta)}{\partial\theta}\right] + \frac{\pi\partial(wv)}{\partial\sigma} - \frac{\pi uu\tan\theta}{a} - \pi uf - \frac{1}{a}\left[\pi\frac{\partial\phi}{\partial\theta} + RT\frac{\partial\pi}{\partial\theta}\right] + \pi F_v + D_v \qquad (2)$$

Thermodynamic equation

$$\frac{\partial \pi T}{\partial t} = -\frac{1}{a \cos\theta}\left[\frac{\partial(\pi u T)}{\partial \lambda} + \frac{\partial(\pi v T \cos\theta)}{\partial \theta}\right] + \frac{\pi \partial(wT)}{\partial \sigma}$$

$$+ \frac{RT}{C_p \sigma}\left[-w\pi + \sigma\left(\frac{\partial \pi}{\partial t} + \frac{1}{a \cos\theta}\left[u\frac{\partial \pi}{\partial \lambda} + v\frac{\partial \pi}{\partial \theta}\cos\theta\right]\right)\right]$$

$$+ \pi H + D_T \qquad (3)$$

Moisture continuity equation

$$\frac{\partial q\pi}{\partial t} = -\frac{1}{a \cos\theta}\left[\frac{\partial(\pi u q)}{\partial \lambda} + \frac{\partial(\pi v q)}{\partial \theta}\right]$$

$$+ \frac{\pi \partial(wq)}{\partial \sigma} + \pi Q + Dq \qquad (4)$$

Mass continuity equation

$$\frac{\partial \pi}{\partial t} = -\frac{1}{a \cos\theta}\left[\frac{\partial(u\pi)}{\partial \lambda} + \frac{\partial(v\pi \cos\theta)}{\partial \theta}\right] + \pi \frac{\partial w}{\partial \sigma} \qquad (5)$$

Hydrostatic equation

$$\frac{\partial \phi}{\partial \sigma} = -\frac{RT}{\sigma} \qquad (6)$$

Equation of state

$$\alpha P = RT \qquad (7)$$

The dimensionless vertical coordinate sigma (σ) is defined as

$$\sigma = \frac{P}{\pi} \ . \qquad (8)$$

The measure of the vertical motion

$$w = -\frac{\partial \sigma}{\partial t} = -\dot{\sigma} \qquad (9)$$

A complete list of symbols and abbreviations used in the above equations may be found in the front of this thesis.

The terrain pressure derivatives appearing as part of the pressure gradient force terms in the momentum equations are computed by a special finite difference scheme in order to reduce the truncation error noted by Kurihara (1968). Even though the main purpose of this scheme is to correct problems occurring over steep terrain, it was allowed to remain in the model during the experiments reported in this thesis in which a flat earth (all terrain heights at sea level) was specified. The technique involves the expression of the gradient of terrain pressure as a function of geopotential on pressure and sigma surfaces. Equation (10) illustrates this relationship.

$$\nabla\pi = \frac{1}{a}\left[\frac{1}{\cos\theta}\frac{\partial\pi}{\partial\lambda}\vec{i} + \frac{\partial\pi}{\partial\theta}\vec{j}\right] = \frac{\pi}{RT}\left[\nabla\phi_p - \nabla\phi_\sigma\right] \qquad (10)$$

The subscript p represents a pressure surface and the subscript σ represents a σ surface. The finite difference scheme given in Appendix A utilizes this relationship by interpolating the value of the geopotential at adjacent grid points to the pressure surface of the computational grid point and then performing the integration on a pressure surface. The computational grid point is common to a sigma surface and the pressure surface on which the integration takes place. Thus, pressure force is computed at a point on the sigma surface.

The terrain pressure derivatives appearing in the thermodynamic equation as part of the term representing the work done per unit time and mass by the pressure force are also handled in a special way as shown in Appendix A.

B. SPHERICAL COORDINATES, STAGGERED GRID

The spherical grid points occur at five degree intervals of latitude and longitude. These grid points are subdivided into two categories; mass points at which the mass variables π, ϕ, T, q, and w are retained and velocity points at which the motion variables u and v are carried. The poles are considered mass points. Mass points and velocity points are staggered throughout the grid, hence mass and velocity points occur at ten-degree intervals. Figure (1) taken from Mihok (1974) illustrates the spherical coordinate, staggered grid.

When a variable is needed at a grid point on which it is not carried, an average of the values at the surrounding grid points is taken. For example if π is needed at a velocity point, the average of the π values at the four mass points surrounding the velocity point is used.

C. VERTICAL LAYERS

The atmosphere is vertically divided into five layers in sigma. The variables u, v, T, ϕ are retained at the 0.9, 0.7, 0.5, 0.3 and 0.1 sigma levels, which are the centers of each of the five layers. The specific humidity (q) is retained only in the lower three layers. This is reasonable for the distribution of moisture in the atmosphere. The quantity $w = -\dot{\sigma}$ is carried at the interfaces of the vertical layers (0.8, 0.6, 0.4, 0.2 sigma levels) and is zero at the upper and lower boundaries. Figure 2 provides a graphic description of the vertical atmospheric layering used in the model.

D. SPATIAL FINITE DIFFERENCE METHODS

The experiments in this thesis fall into two categories: (1) experiments comparing second order spatial differencing versus mixed second and fourth order spatial differencing, and (2) experiments examining the reaction of the model to flow over the poles with second order differencing.

1. Second Order and Mixed Second and Fourth Order Finite Differencing

Williams (1972) has shown that phase speed errors with fourth order finite differencing are considerably less than phase speed errors occurring with second order differencing. However, fourth order differencing requires a reduction in the length of the time step in order to insure linear computational stability. (Time step requirements are discussed more fully in Section II-E.) Williams found that the time step would not have to be reduced as much if fourth order differencing is limited to the advection and divergence terms. These terms are the principal ones which affect the phase speeds of the meteorological waves.

In order to gain improved phase speeds for meteorological waves while keeping the necessary reduction of the time step to a minimum, Mihok (1974) inserted a mixed second and fourth order differencing scheme into the model. The mixed scheme is documented in Appendix B.

Another factor affecting the phase speeds of waves in the model is the arrangement of points in the horizontal. Phase speed errors for waves moving along the coordinate axes, with the difference scheme of this thesis, are the same as those for an unstaggered grid. However, Williams (1972) has noted that waves propagating at an angle of 45° to

the coordinate axis will have a larger phase speed error on the staggered grid than on the unstaggered grid. This is because the staggered grid points used in the difference equations are more widely separated relative to a wave that is moving at a 45° angle with respect to the coordinate axes.

2. Polar Finite Differencing

One of the difficult problems associated with spherical coordinates is the treatment of the poles which are singular points. The zonal and meridional wind components are undefined at the poles. In the difference equations for this model any term requiring a velocity component from the poles is set to zero.

Since the poles are considered mass points in this model separate calculations of the mass point parameters (π, T, q, ϕ, w) are made for the poles. Following the procedure of Arakawa (1974), polar mass point parameters in the model change as the result of the meridional mass flux at all velocity points on the 85° latitude circle. The flux at each mass point is weighted to represent a triangular area with apexes located at the pole and at the mass points adjoining the velocity point. When an individual mass point parameter has been calculated for each of the 36 triangular areas surrounding the pole, an average is taken and inserted as the pole value. As an illustration, the equation for the contribution of one atmospheric layer to the local change in terrain pressure can be written

$$\left(\frac{\partial \pi}{\partial t}\right) = \frac{1}{a \cos \theta} < \frac{\Delta u \bar{\pi}}{2\Delta\lambda} + \frac{\Delta(v\bar{\pi} \cos \theta)}{2\Delta\theta} > \qquad (11)$$

where $< >$ indicates a vertical summation of the layer contributions and $\bar{\pi}$ the terrain pressure at a velocity point obtained by averaging the π values at the four surrounding mass points.

By clearing all terms from the denominator of (11) and multiplying by the earth's radius, a , one can obtain

$$\left(\frac{\partial \pi}{\partial t}\right) [a^2 4\Delta\lambda\Delta\theta \cos\theta] = < \Delta u\bar{\pi}\, a2\Delta\theta + \Delta(v\bar{\pi} \cos\theta)a2\Delta\lambda > \qquad (12)$$

The quantity on the left hand side, $[a^2 4\Delta\lambda\Delta\theta \cos\theta]$, represents the approximate area of a ten-degree square with a velocity point at its center. The u and v values at the central velocity point control the flux over the area. The triangular flux areas surrounding the pole are one quarter the size of the square flux areas at lower latitudes. Thus, the equation for each polar triangular flux area becomes

$$\left(\frac{\partial \pi}{\partial t}\right) [a^2 \Delta\lambda\Delta\theta \cos\theta] = [\pm < v\bar{\pi} \cos\theta > a^2 \Delta\lambda] \qquad (13)$$

All mass flux terms except the meridional flux along the 85° latitude circle are omitted .

The following equation shows how the contribution of each of the 36 flux triangles is averaged to obtain the final value for the local change in terrain pressure at the pole.

$$\left(\frac{\partial \pi}{\partial t}\right) = \frac{2}{a\Delta\theta} \frac{1}{36} \sum_{n=1}^{36} \pm < \bar{\pi}v > \qquad (14)$$

An experiment was also performed using values at the poles obtained solely from averaging the desired quantity around the 85° latitude circle. This method is much simpler to apply and requires less computer time.

Another problem which occurs near the polar region is maintaining computational stability as the meridians converge to the poles and the

grid distance along a latitude circle steadily decreases. Since it is not desirable to reduce the time step or modify the grid Arakawa's (1974) method of smoothing the zonal component of the pressure gradient force and the divergence is used. A stability coefficient, given in the following Equation (15) is used to determine the smoothing.

$$S = \frac{D \cos \theta}{C_o \, \Delta t \sin (md)} \qquad (15)$$

where

S = stability coefficient

D = 5° grid distance at equator

C_o = phase speed of the fastest gravity wave

Δt = time step

m = wave number

d = 5° in radians

If the value of S is less than 1 smoothing is necessary. The field to be smoothed is expanded into a Fourier series and the amplitude of each unstable wave component is reduced by a factor proportional to S. Arakawa states that this method of smoothing does not smooth the fields of variables because it is simply a generator of multiple point difference quotients.

Several of the experiments with flow over the pole involved modification of the stability coefficient or direct smoothing of the main variables in addition to the zonal pressure gradient and divergence fields.

E. TIME FINITE DIFFERENCE METHODS

The initial time step in the model is performed using the Euler backward (Matsuno) difference scheme which is expressible as follows:

$$F^{*} = F^{t} + \Delta t \frac{\partial F^{t}}{\partial t} \text{ [first approximation]}$$

$$F^{t+1} = F^{t} + \Delta t \frac{\partial F^{*}}{\partial t} \text{ [forecast] .} \qquad (16)$$

F is a vector including the dependent variable, the superscript t denotes the time step, the superscript * indicates the result of the intermediate step and Δt is the time interval of a single time step. The Euler backward scheme is a two step iterative scheme which is either damping or neutral depending on the wave number (Haltiner and Williams, 1973). The principal damping takes place in short waves. For this reason the Euler backward scheme is applied at three-hour intervals in addition to the initial application.

All other time steps are performed using central differences, commonly called the leapfrog scheme;

$$F^{t+1} = F^{t-1} + 2\Delta t \frac{\partial F^{t}}{\partial t} \qquad (17)$$

The leapfrog scheme gives rise to a spurious wave called the computational mode which has no counterpart in the analytic solution to the differential equation. The phase of the computational mode changes every time step causing the solutions at even and odd time steps to decouple. The amplitude of the computational mode is greatest for short wavelengths (Haltiner, 1971).

In order to limit the effects of the computational mode and reduce noise in the short wavelengths the Euler backward scheme is applied every three hours. As previously mentioned, this tends to dampen short waves somewhat. In addition, it is important to note that there is no computational mode associated with the Euler backward scheme and therefore application of this scheme recouples the solution.

A time step of ten minutes is used when second order differencing is applied throughout the model. When the mixed second and fourth order differencing scheme (Williams, 1972), (Mihok, 1974) is used the time step is reduced to eight minutes. Williams showed, experimenting with the linearized barotropic primitive equations, that a 14% smaller time step was needed with mixed second and fourth order spatial differencing in order to meet the von Neumann necessary condition for stability. Both the ten-minute and eight-minute time steps are too large near the poles to maintain stability unless Arakawa's method of smoothing derivatives is used.

III. INITIALIZATION

Initial conditions for all experiments in this thesis were derived analytically. They approximate an initial barotropic state. Generation of initial conditions in this study differs from the method used by Elias (1973) and Mihok (1974) in that an analytic solution for ϕ rather than a numerical solution of the balance equation is used. Generation of initial conditions in this manner was found to be less time consuming and produced waves with almost no noise that propagated with small distortion.

Initial temperatures are generated on twelve constant pressure levels distributed from 1000 mb to 50 mb and height values are generated for ten of these levels. In addition, sea level pressure and sea surface temperature fields are produced. Wind fields are generated at seven constant pressure levels. All generated fields are interpolated to sigma surfaces. Initial values at the poles are averages taken around the 85° latitude circle on sigma surfaces.

A. ANALYTIC BALANCING

The initial geopotential and velocity fields used for the experiments in this thesis were obtained from the stream function solution to the linearized vorticity equation (Haurwitz, 1940).Neamtan (1946) later solved the complete vorticity equation and obtained results verifying Haurwitz's work.

The expression for the stream function, ψ , is given by

$$\psi = A^* \sin(m\lambda - \nu t) \sin\theta \cos m\theta - B a^2 \sin\theta \qquad (18)$$

where m is the wave number, ν is the angular wave velocity, a is the radius of the earth and A^* and B are constants. The amplitude constant, A^* , (Elias, 1973) is defined as

$$A^* = A\,[(2m!/2^N N!)] \quad , \qquad (19)$$

where $N = m+1$ and A is a constant. The constant B is directly related to the angular phase speed by the equation

$$\frac{\nu}{m} = B\,\frac{N(N+1) - 2}{N(N+1)} - \frac{2\Omega}{N(N+1)} \qquad (20)$$

where (ν/m) is the angular phase speed, and Ω is the angular velocity of the earth.

Haurwitz (1940) has shown that harmonic waves defined by this stream function in a barotropic non-divergent atmosphere will move with a constant angular velocity without changing shape. Harmonic waves generated in this way provide excellent controlled conditions for testing and debugging atmospheric models. Many experimenters including Phillips (1959), Gates (1962), Heburn (1972), Holloway, Spelman,and Manabe (1973), Elias (1973), and Mihok (1974) have used the Haurwitz stream function to generate initial conditions.

It should be noted that the equations used in the model are not those of a non-divergent atmosphere. Phillips (1959) has noted that the presence of divergence in the barotropic atmosphere will slow the rate

of progression of the flow pattern especially for small values of the wave number m.

The Haurwitz stream function is used by Phillips (1959) as the forcing function to obtain the geopotential from the non-linear balance equation

$$\nabla^2\phi = f\nabla^2\psi - \nabla\psi \cdot \nabla f - 2\left(\frac{\partial^2\psi}{\partial x\partial y}\right)^2 + 2\left(\frac{\partial^2\psi}{\partial x^2}\frac{\partial^2\psi}{\partial y^2}\right) \tag{21}$$

Equation (21) in spherical coordinates becomes

$$\frac{1}{a^2}\left[\frac{1}{\cos^2\theta}\frac{\partial^2\phi}{\partial\lambda^2} + \frac{1}{\cos\theta}\frac{\partial}{\partial\theta}\left(\cos\theta\frac{\partial\phi}{\partial\theta}\right)\right] =$$

$$\frac{f}{a^2}\left[\frac{1}{\cos^2\theta}\frac{\partial^2\psi}{\partial\lambda^2} + \frac{1}{\cos\theta}\frac{\partial}{\partial\theta}\left(\cos\theta\frac{\partial\psi}{\partial\theta}\right)\right] + \frac{1}{a^2}\frac{\partial\psi}{\partial\theta}\frac{\partial f}{\partial\theta}$$

$$- 2\left(\frac{1}{a^2\cos\theta}\frac{\partial^2\psi}{\partial\lambda\partial\theta}\right)^2 + \frac{2}{a^4\cos^2\theta}\frac{\partial^2\psi}{\partial\lambda}\frac{\partial^2\psi}{\partial\theta} \tag{22}$$

The solution for ϕ of the non-linear balance equation may be stated as

$$\phi = a^2A(\theta) + a^2B(\theta)\sin m\lambda + a^2C(\theta)(2\sin^2 m\lambda - 1) \tag{23}$$

where ϕ is the geopotential perturbation

$$A(\theta) = \frac{B}{2}(2\Omega + B)\cos^2\theta + \frac{1}{4}\left(\frac{A^*}{a^2}\right)^2\cos^{2m}\theta\left[(m+1)\cos^2\theta + (2m^2-m-2) - \frac{2m^2}{\cos^2\theta}\right], \tag{24}$$

$$B(\theta) = \frac{2(\Omega+B)\,\frac{A^*}{a^2}}{(m+1)(m+2)} \cos^m \theta \left[(m^2 + 2m+2) - (m+1)^2 \cos^2 \theta\right] \qquad (25)$$

and

$$C(\theta) = \frac{1}{4} \left(\frac{A^*}{a^2}\right)^2 \cos^{2m} \theta \left[(m+1) \cos^2 \theta - (m+2)\right] \qquad (26)$$

This solution was obtained by Phillips (1959). Equation (23) provides a geopotential perturbation field. The height at a particular pressure level is obtained by adding the height perturbation from (23) to the mean height for that level obtained from the NACA standard atmosphere (Haltiner and Martin, 1957).

The linear balance equation may be obtained by dropping the last two terms in (21) for Cartesian coordinates and (22) for spherical coordinates. The linear solution is given by

$$\phi = F(\theta) + G(\theta) \sin (m\lambda - \nu t) \qquad (27)$$

where

$$F(\theta) = B\Omega a^2 \cos^2 \theta \qquad (28)$$

and

$$G(\theta)\sin(m\lambda-\nu t) = A^* 2\Omega\left[\frac{m^2 + 2m + 2}{(m+1)(m+2)}\right] \sin(m\lambda-\nu t) \cos^m \theta$$

$$- A^*\Omega \frac{2(m+1)}{(m+2)} \sin (m\lambda - \nu t) \cos^{m+2} \theta \qquad (29)$$

The solution to the linear balance equation produces initial fields which are in geostrophic equilibrium while the non-linear solution produces fields which are in approximate gradient equilibrium and therefore more realistic. This is especially true near the equator where the geostrophic approximation is invalid. For this reason non-linear balancing is used in all experiments in this thesis except Experiment 3 which involves a flow pattern of wave number 12.

In Experiment 3,non-linear balancing results in aliasing, (Haltiner, 1971), which distorts the initial fields. This problem was eliminated by the use of linear balancing. The effect of eliminating the non-linear terms is minimal because the wave amplitude used in the experiments is small.

B. ANALYTIC WINDS

Analytic zonal and meridional wind components are obtained from the derivatives

$$u = -\frac{1}{a}\frac{\partial \psi}{\partial \theta} \tag{30}$$

and

$$v = \frac{1}{a \cos \theta}\frac{\partial \psi}{\partial \lambda} \quad . \tag{31}$$

The results are

$$u = -\frac{1}{a}[A^{*}\sin(m\lambda-\nu t)\cos^{m+1}\theta - mA^{*}\sin(m\lambda-\nu t)\cos^{m-1}\theta\sin^{2}\theta - Ba^{2}\cos\theta] \tag{32}$$

$$v = \frac{1}{a}[A^{*}m \sin\theta \cos^{m-1}\theta \cos(m\lambda - \nu t)] \quad . \tag{33}$$

C. ANALYTIC TEMPERATURES

Analytic temperatures, constant on each pressure surface, are generated in accordance with the National Advisory Committee for Aeronautics (NACA) standard atmosphere (Haltiner and Martin, 1957).

IV. RESULTS

The experiments conducted for this thesis fall into two categories: (1) experiments comparing second order differencing versus mixed second and fourth order differencing as discussed in Section II-D-1 and (2) experiments attempting to improve the forecast effectiveness of the model when there is flow over the poles.

In all experiments presented in this thesis analytically derived fields are used as described in Section III. The variation in the character of the initial harmonic waves was accomplished by varying the specification of the wave number, phase speed and the amplitude constant A which is part of the coefficient A^* given in Equation (19).

The use of analytic fields resulted in the elimination of spurious inertial-gravity waves resulting from initial inconsistencies between the ψ and ϕ fields. Thus, results directly related to the finite differencing of the primitive equations can be examined under controlled conditions without distortion due to initialization.

Surface pressure analysis and forecasts are used to illustrate the output of the model. These analyses, for the Northern Hemisphere only, were obtained by interpolating the spherical grid onto the standard 63 x 63 polar stereographic grid used by FNWC. The interpolation of the spherical data field for a point on the 63 x 63 grid is accomplished by using the Ayres' central difference formula, which is continuous in the first derivative. If the point lies within the border zone, a double linear interpolation is performed. Very little detail is lost, except at the pole as shall be shown in Experiment VIII.

Harmonic analysis (Jeffreys and Jeffreys, 1956) is performed on the surface pressure analysis and on the forecasts at three-hour intervals. The harmonic analysis reveals the wave numbers present around a latitude circle and their amplitudes and phases.

A. SECOND ORDER DIFFERENCING VERSUS MIXED SECOND AND FOURTH ORDER DIFFERENCING

Experiment I. In this experiment, wave number 6, a phase speed of + 12° longitude per day and A = 1000 are used. Chart A shows the initial surface pressure field. Chart B is the 48-hour forecast using second order differencing and Chart C shows the 48-hour forecast using the mixed differencing scheme. Note that the forecast fields retain their definition and are not distorted by undesirable inertial gravity waves. Figure 3 shows the phase angles in degrees longitude as a function of latitude at 12-hour intervals to 48 hours for second order differencing. Figure 4 shows the same relationship for the mixed differencing scheme. Comparison of Figures 3 and 4 shows a considerable improvement in the forecast phase speed of the waves when the mixed differencing scheme is used. This is especially true as the latitude increases. Above 60^{o} latitude the mixed scheme forecasts of phase speed are too fast while the second order forecasts indicate a greatly retarded phase speed.

Experiment II. Wave number 9, a phase speed of + 12° longitude per day and A = 0.1 are used in this experiment. Chart D shows the initial surface pressure field. Chart E is the 48-hour forecast using second order differencing. Chart F is the 48-hour forecast using the mixed differencing scheme. The forecast and initial fields are not distorted

by undesirable gravity waves. Figure 5 shows the phase angles in degrees longitude as a function of latitude at 12-hour intervals out to 48 hours for second order differencing. Figure 6 shows the same relationship for the mixed differencing scheme. Comparison of Figures 5 and 6 indicates a closer approximation to the true phase speed when the mixed scheme is used. Above 60° latitude the mixed scheme phase speeds are too fast while considerable slowing is evident for second order differencing.

Experiment III. Wave number 12, a phase speed of + 12° longitude per day and $A = 5 \times 10^{-6}$ are used in this experiment. The initial surface pressure field is shown in Chart G while Charts H and I are the 48-hour forecast fields for the second order differencing and mixed differencing schemes, respectively. Note that the initial and forecast fields are not distorted by gravity waves. Figure 7 shows the phase angles in degrees longitude as a function of latitude at 12-hour intervals out to 48 hours for second order differencing while Figure 8 shows the same relationship for the mixed differencing scheme. When the second order differencing is used there is very little wave propagation. The phase progression is very distorted and marked retrogression is noted above 40° latitude. Figure 8 indicates a distinct improvement in the propagation of the waves when the mixed differencing scheme is employed. In Figure 8 the phase speed of the waves increases with latitude. However, at all latitudes the phase speeds are slower than for the nondivergent analytic solution.

It should be noted that the solution to the linear balance equation was used to generate the initial height fields in this case. The use of the non-linear solution resulted in undesirable aliasing.

B. CROSS-POLAR FLOW

McCollough (1974) remarked that "noise" developed in the polar regions as the forecast time progressed and that longer integrations indicated a need for a review of the polar region finite differencing and the method of handling the pole point. In order to examine the effectiveness of the model in forecasting for the polar regions, flow over the poles was generated analytically using wave number 1 and a phase speed of -94.4° longitude per day. After some experimentation it was decided to make $A = 3 \times 10^7$ yielding a maximum wind of 20 kts in the polar region. This method of generating cross-polar flow was taken from Holloway, Spelman and Manabe (1973).

Chart J is the initial surface pressure analysis used for the flow over the pole experiments. Charts K-N illustrate surface pressure forecasts at 12-hour intervals out to 48 hours. All cross polar flow experiments use second order differencing.

Examination of Chart J reveals that the isobars are evenly spaced and curve smoothly over the pole. However, the pattern of the isobars becomes increasingly distorted near the pole with progressive forecasts as can be seen in Charts K-N. The objective of the subsequent experiments is to test various modifications to the model in order to improve the accuracy of forecasts in the polar region when cross-polar flow is present.

Experiment IV. Based on the assumption that the distorted flow pattern in the polar regions was the result of errors in the derivatives near the pole, smoothing of the derivatives was increased by squaring the stability coefficient, S , defined in Equation (15). This

modification did not result in smoother forecasts in the polar regions and in fact the disturbance was slightly augmented as can be seen by a comparison of Chart L and Chart O.

Experiment V. In this experiment removal of the irregularities in the polar region was attempted by applying the Arakawa smoothing technique directly to the main variables at three-hour intervals. The Arakawa smoothing was applied to π, u, v, T and q on the ninth and tenth time steps after the Matsuno step. Charts P and Q are the 24-hour and 48-hour forecasts made with this technique. Comparison of the above charts with Charts L and N reveal a reduction in the amplitude of the disturbance at the pole and a more uniform flow at the higher latitudes.

Experiment VI. The promising results of Experiment V made it seem probable that application of Arakawa smoothing to the main variables at every time step would totally remove the distortion of the isobars near the pole. Although this method gave somewhat improved results over the case where the main variables were not smoothed, the effect was still not as good as that achieved in Experiment V.

Experiment VII. Holloway, Spelman and Manabe (1973) transformed vector components into a polar stereographic mapping prior to Fourier filtering in order to prevent excessive smoothing of flow over the pole. Their Fourier filtering method is similar to the Arakawa smoothing technique except that the shorter waves are completely removed. In this experiment the main variables were smoothed every three hours, as in Experiment V; but prior to smoothing, the wind components u and v were transformed to a polar stereographic projection plane. The method of transformation is the same as used by Holloway, Spelman and Manabe.

This experiment resulted in the model becoming unstable after 27 hours.

Experiment VIII. At this point in the experimentation it was noted that the interpolation technique used to transform the surface pressure field from spherical coordinates to a 63 x 63 polar stereographic grid was not adequately handling the pole point. Hence, the interpolation scheme was bypassed at the pole and the pole value on the spherical grid was inserted directly onto the 63 x 63 grid which is centered at the pole. Chart R and S show the result of this modification of the output interpolation scheme. The flow appears to be smoother indicating that a portion of the distortion in the polar regions was due to a faulty output interpolation scheme.

Experiment IX. This experiment tests the effect of using only averages around the 85° latitude circle for values needed at the poles. The modified output interpolation scheme (Experiment VIII) is included in the model for this experiment. The resulting 24-hour forecast is shown in Chart T which shows a considerable improvement over Chart L (the original cross-polar flow 24-hour forecast). However, there is little difference between the 24-hour forecast using just the modified output interpolation scheme (Experiment VIII, Chart S) and Chart T which includes the additional feature of using averages for polar parameters.

Experiment X. This experiment consisted of a combination of the modified output interpolation scheme (Experiment VIII) and the application of Arakawa smoothing to the main variables at three-hour intervals (Experiment V). Chart U shows that Arakawa smoothing of the main variables at three-hour intervals reduces the distortion at the pole by a considerable amount. The improvement was larger than in Experiment V.

A 48-hour forecast was not produced in this experiment due to time limitations.

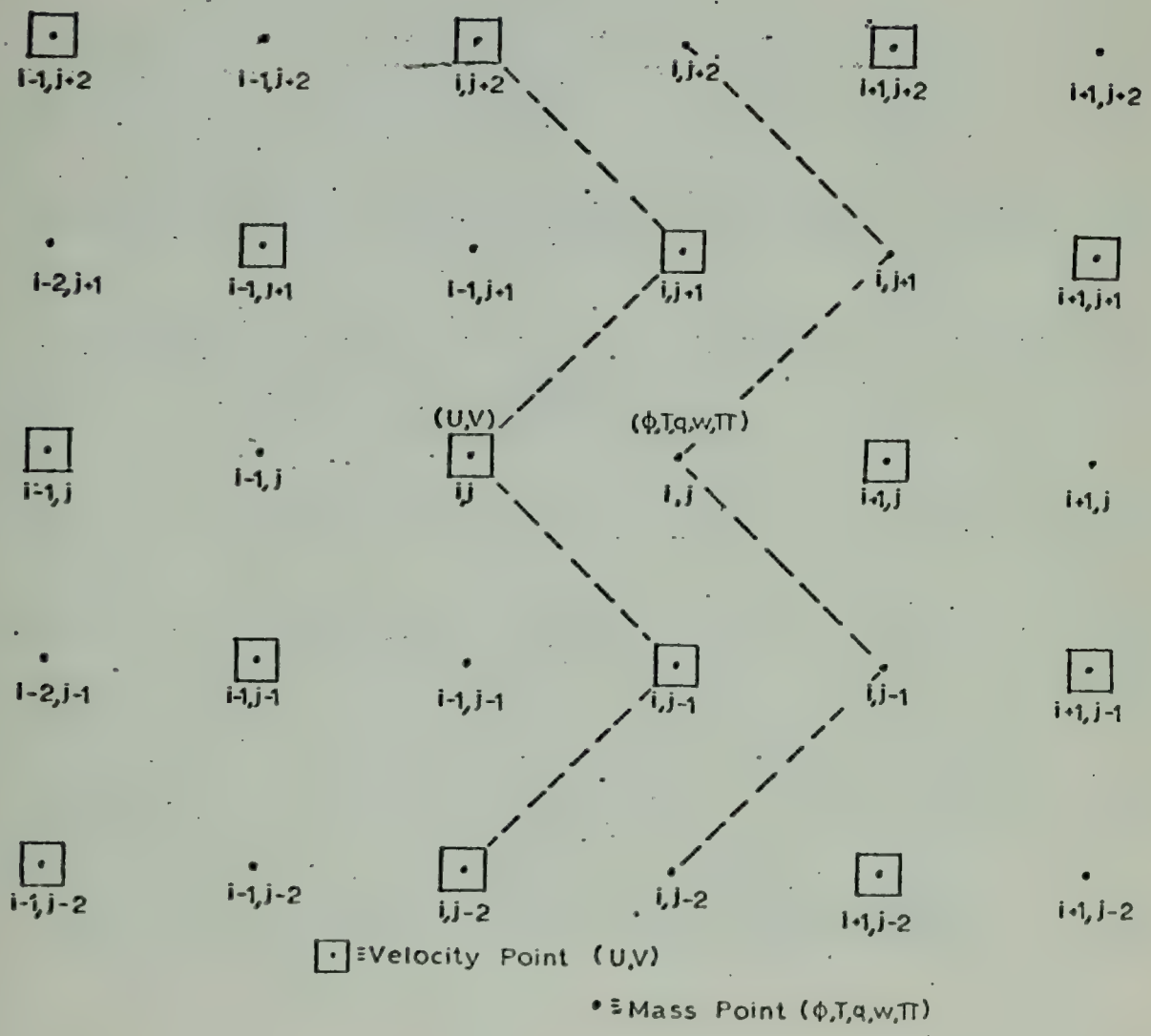

FIGURE 1. LOCATION OF VARIABLES.

i is the column counter and j is the row counter.
Point (1,1) is at 85S, 10E.

Pressure	Computed Variables (at each level)	Level (Notational Subscript)	Sigma (σ)
0.0	w = 0	UPPER BOUNDARY	0.0
.1 × π	u,v,T,ϕ	5	0.1
.2 × π	w	4	0.2
.3 × π	u,v,T,ϕ	4	0.3
.4 × π	w	3	0.4
.5 × π	u,v,T,ϕ,q	3	0.5
.6 × π	w	2	0.6
.7 × π	u,v,T,ϕ,q	2	0.7
.8 × π	w	1	0.8
.9 × π	u,v,T,ϕ,q	1	0.9
π	w = 0	LOWER BOUNDARY	1.0

FIGURE 2. VERTICAL LAYERING

In the above figure, sigma (σ) is the dimensionless vertical coordinate, u and v are the zonal and meridional wind components, respectively, q is the specific humidity, ϕ is the geopotential, π is the terrain pressure and w is the vertical velocity ($-\dot{\sigma}$).

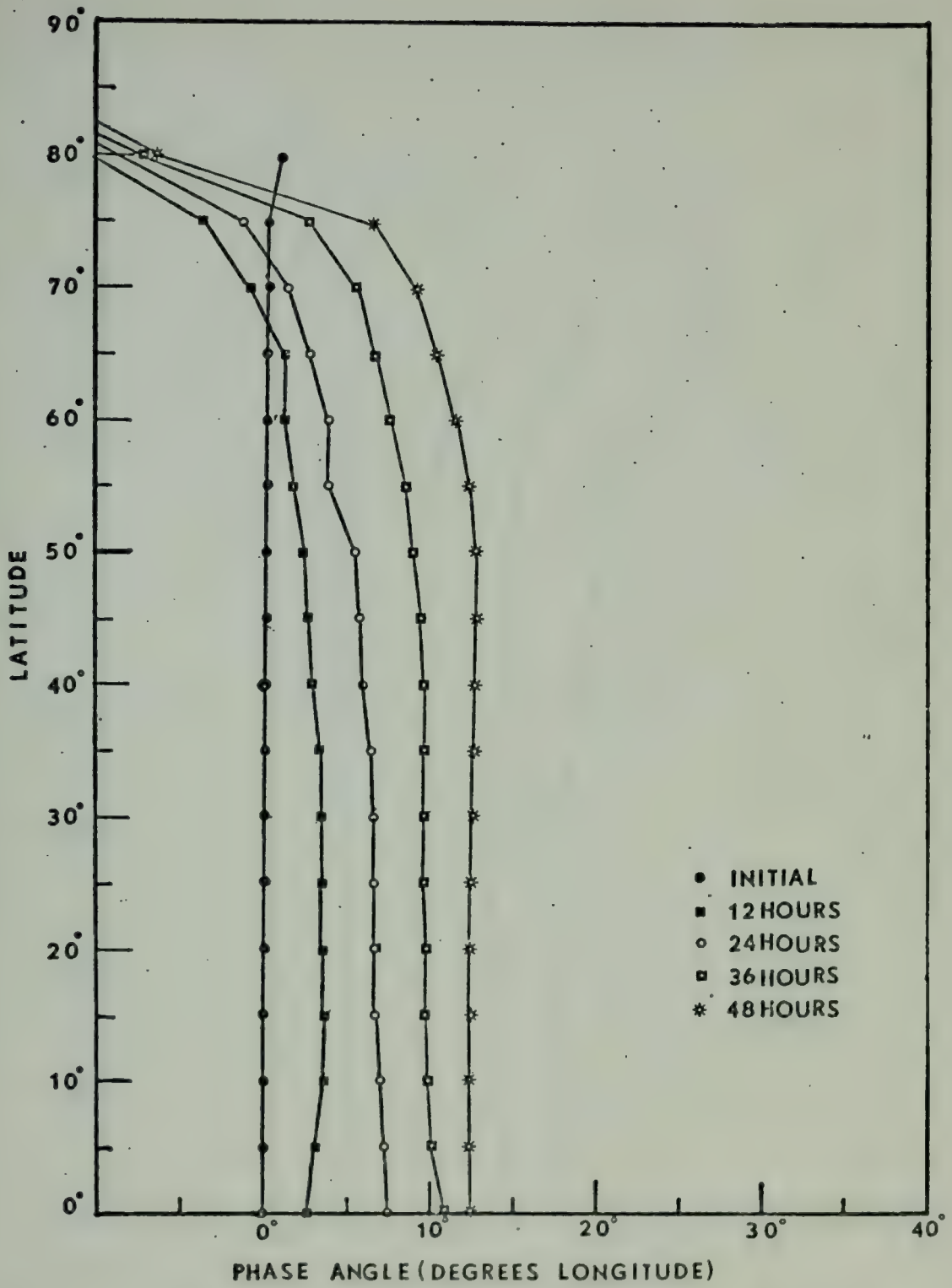

Figure 3. Phase angle (degrees longitude) vs latitude for second order differencing, wave number 6, phase speed 12°/day, A = 1000. (Latitudes with zero wave amplitude are not included.)

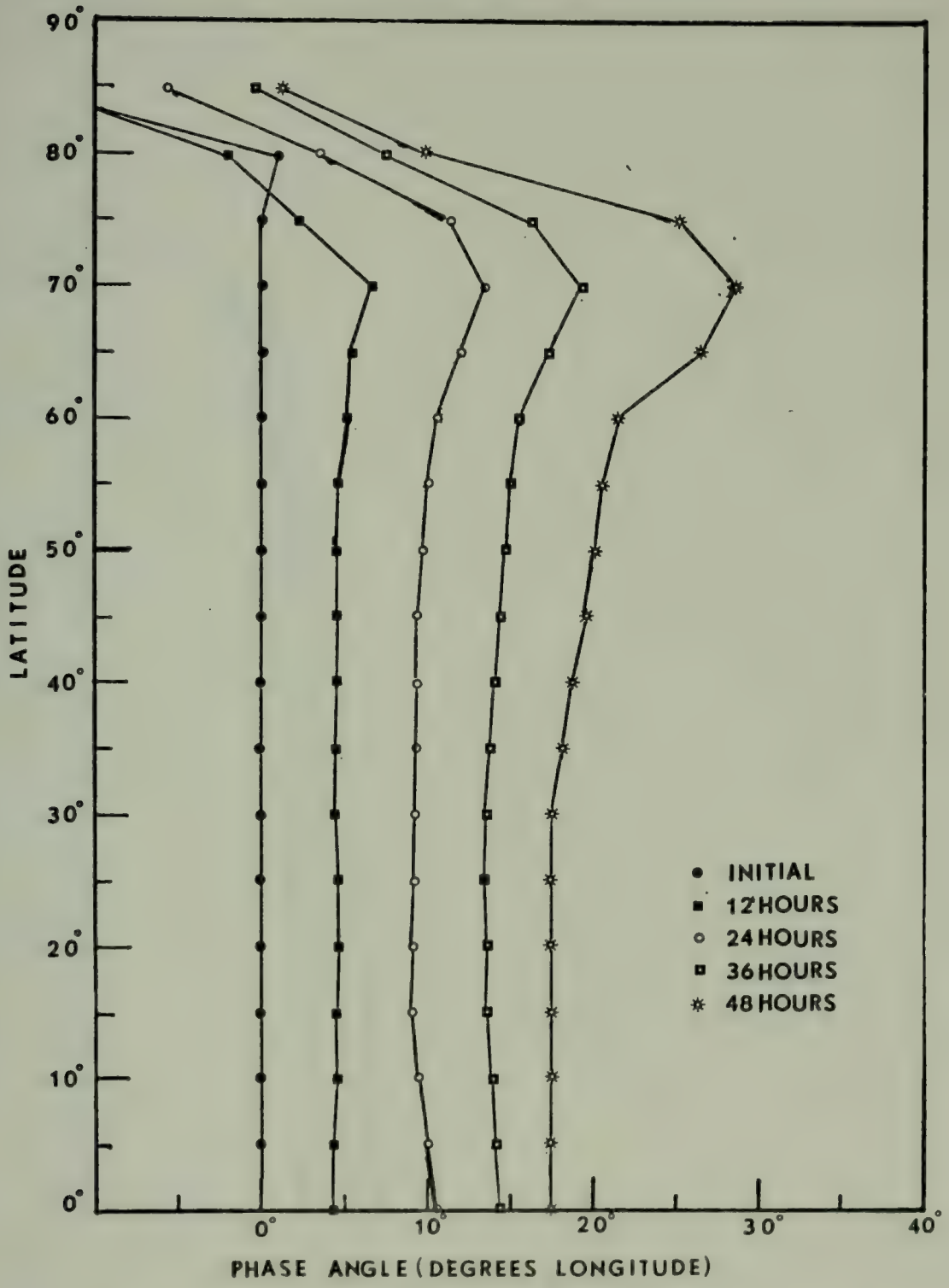

Figure 4. Phase angle (degrees longitude) vs latitude for mixed second and fourth order differencing for wave number 6, phase speed 12°/day, A = 1000. (Latitudes with zero wave amplitude are not included.)

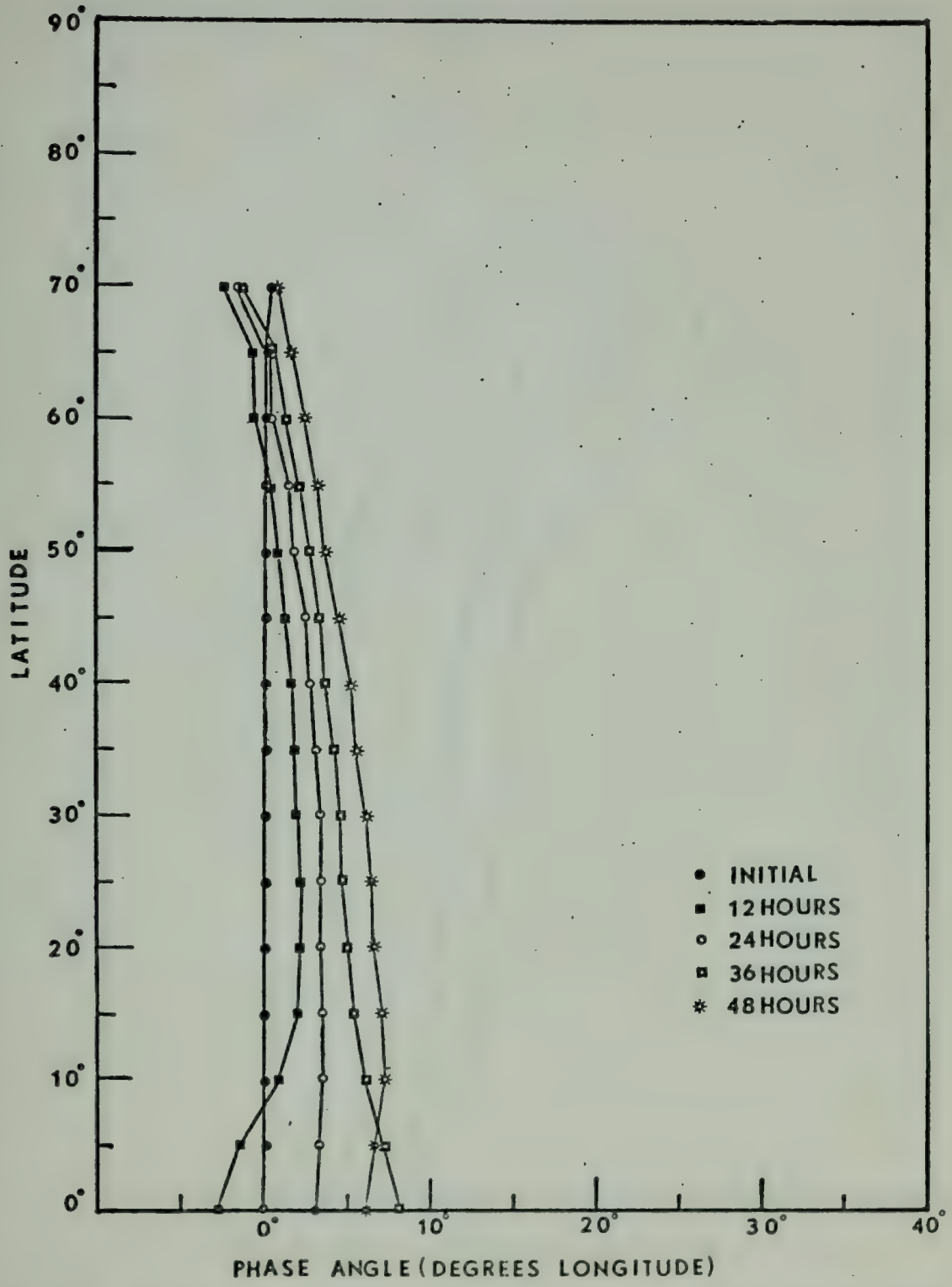

Figure 5. Phase angle (degrees longitude) vs latitude for second order differencing, wave number 9, phase speed 12°/day, A = 0.1. (Latitudes with zero wave amplitude are not included.)

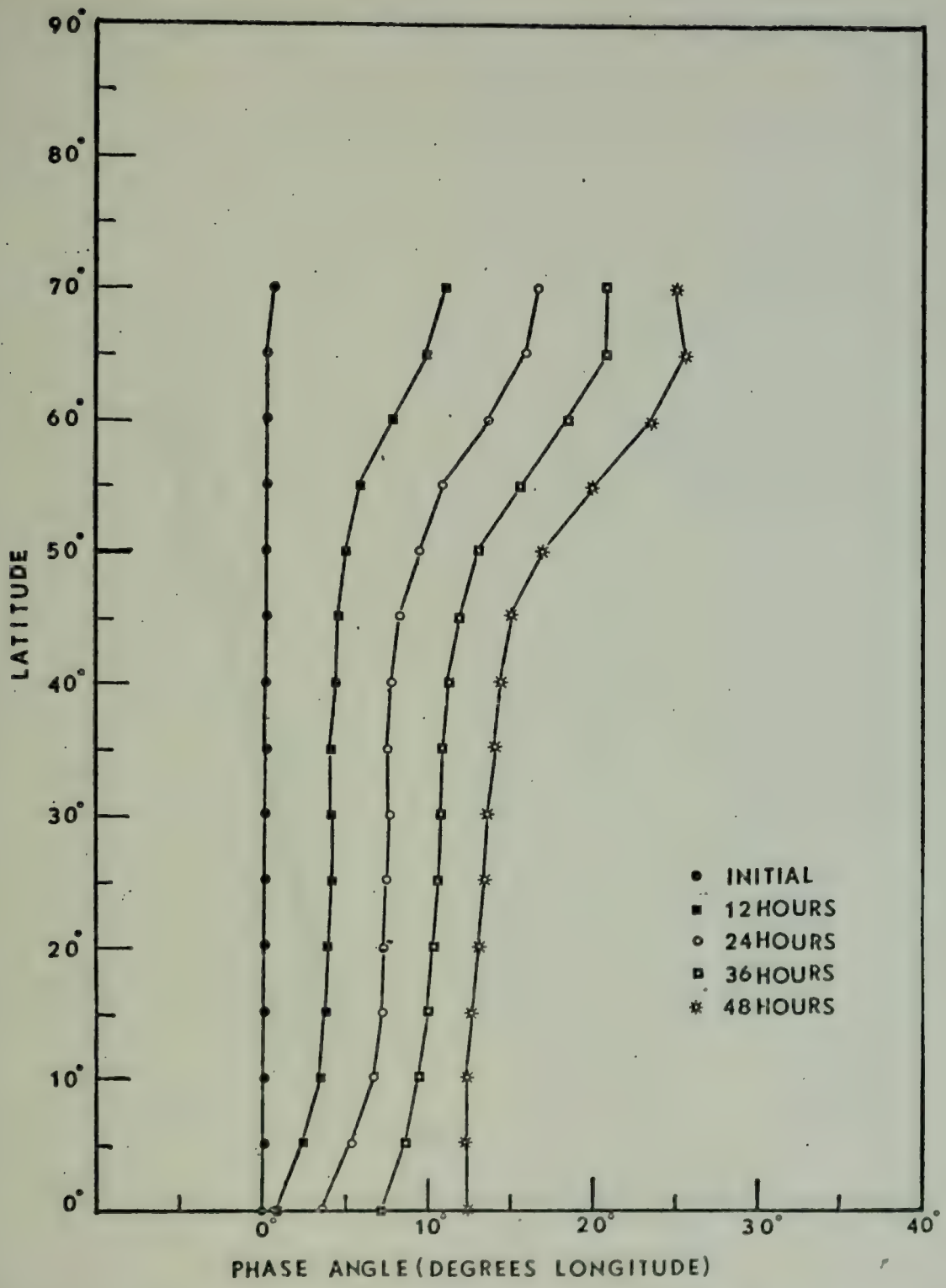

Figure 6. Phase angle (degrees longitude) vs latitude for mixed second and fourth order differencing, wave number 9, phase speed 12°/day, A = 0.1. (Latitudes with zero wave amplitude are not included.)

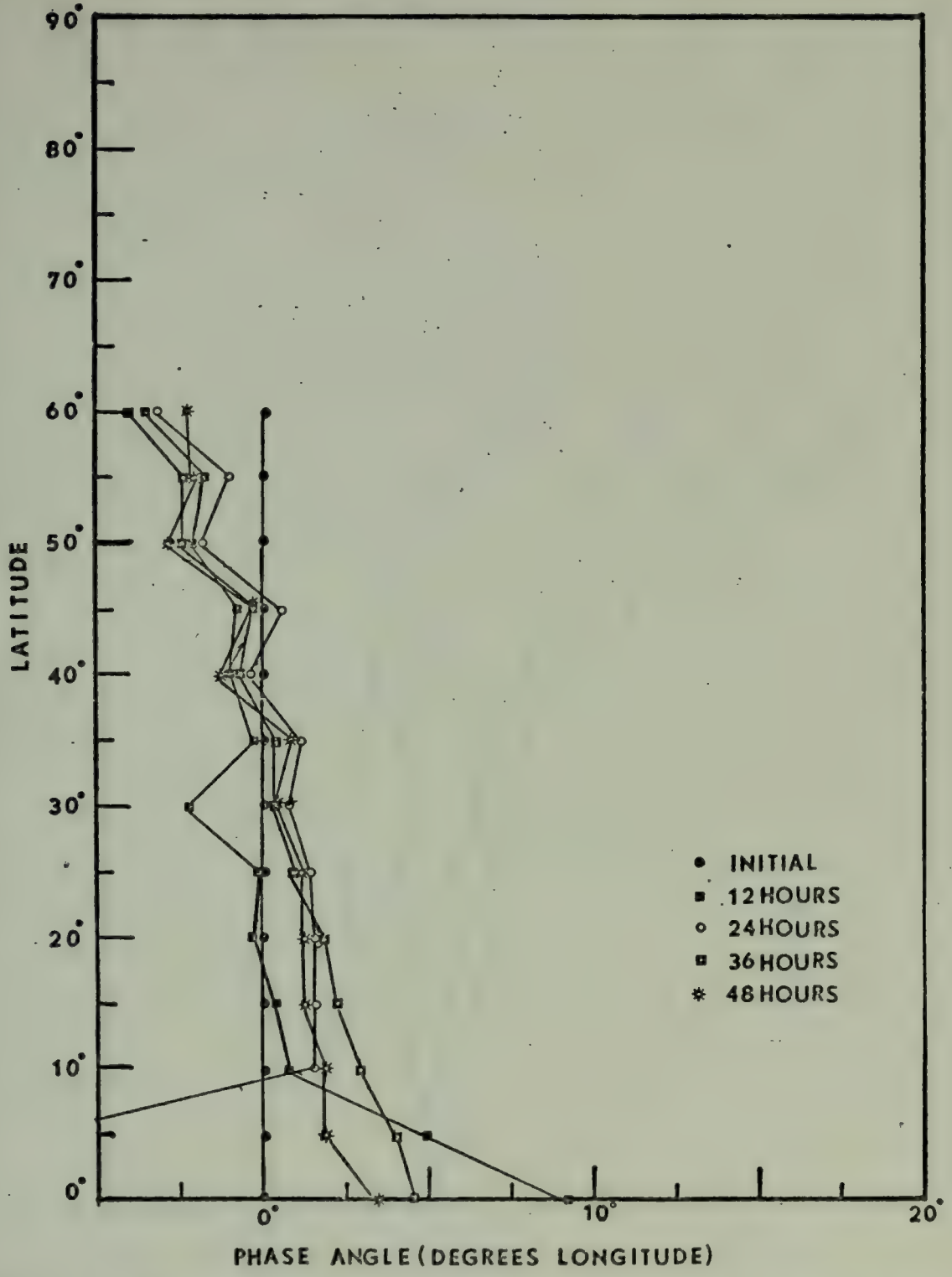

Figure 7. Phase angle (degrees longitude) vs latitude for second order differencing, wave number 12, phase speed 12°/day, $A = 5 \times 10^{-6}$. (Latitude with zero wave amplitudes are not included.)

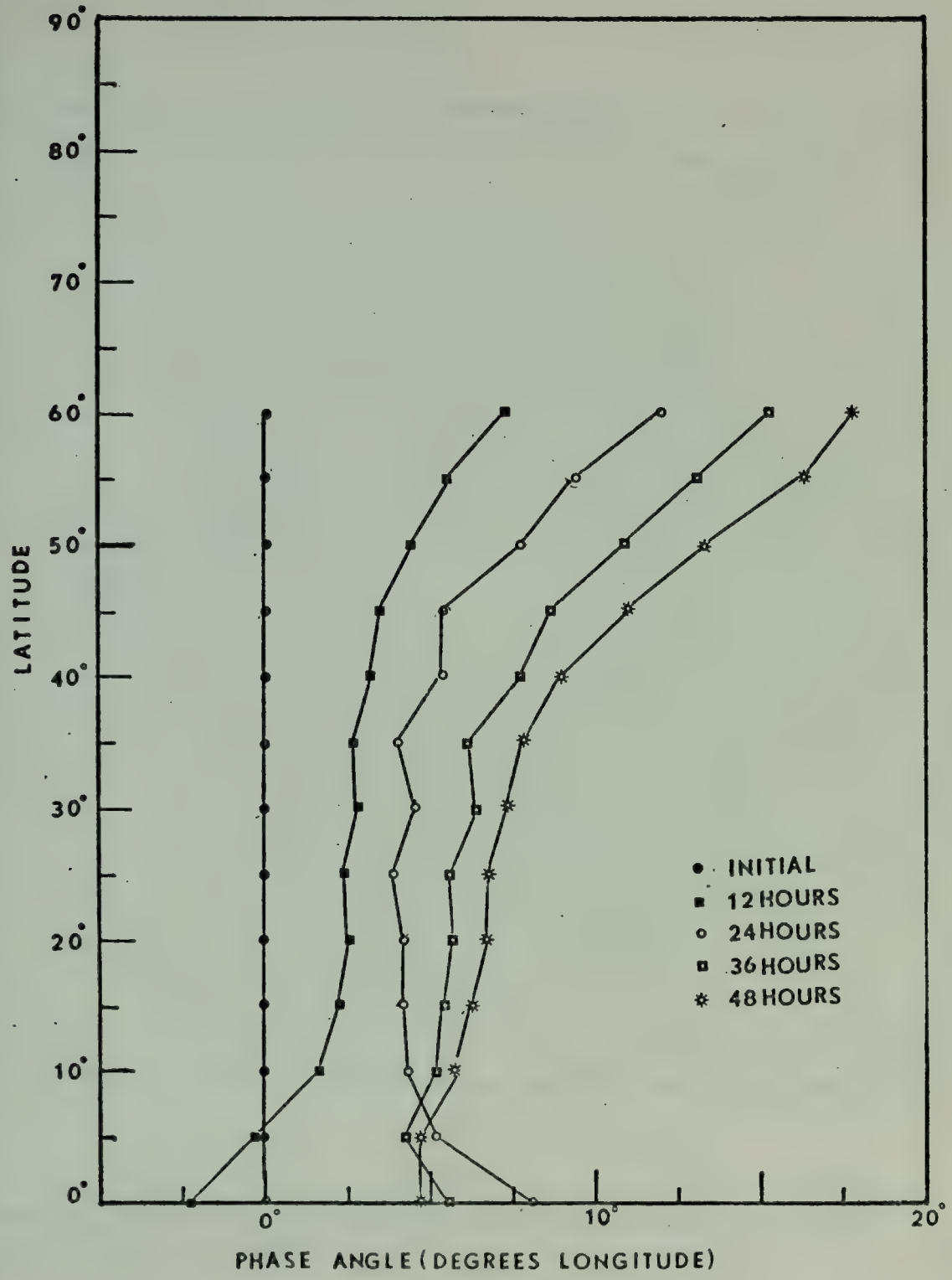

Figure 8. Phase angle (degrees longitude) vs latitude for mixed second and fourth order differencing, wave number 12, phase speed 12°/day, $A = 5 \times 10^{-6}$. (Latitudes with zero wave amplitudes are not included.)

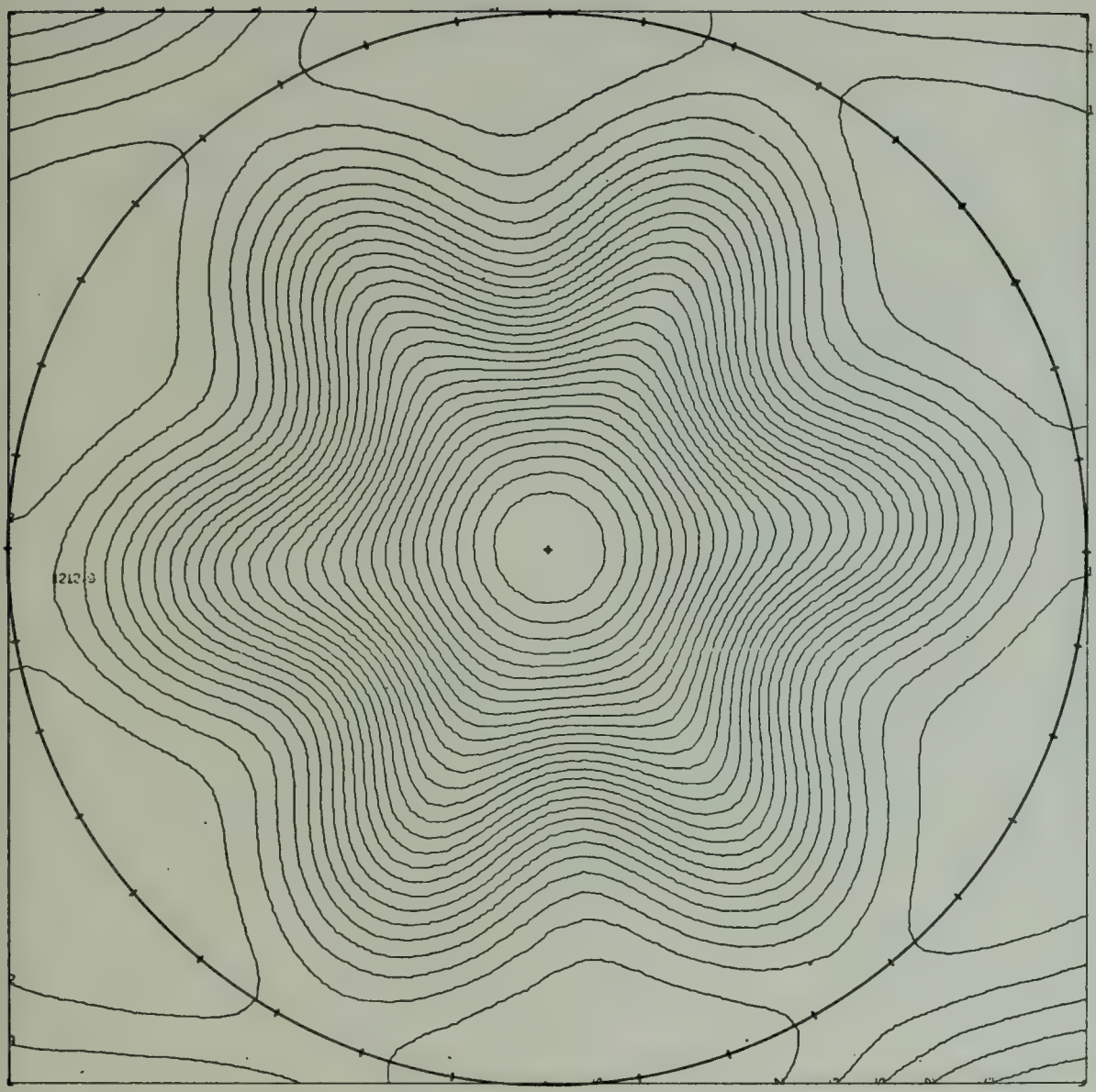

Chart A. Initial surface pressure analysis, wave number 6, phase speed 12°/day, A = 1000.

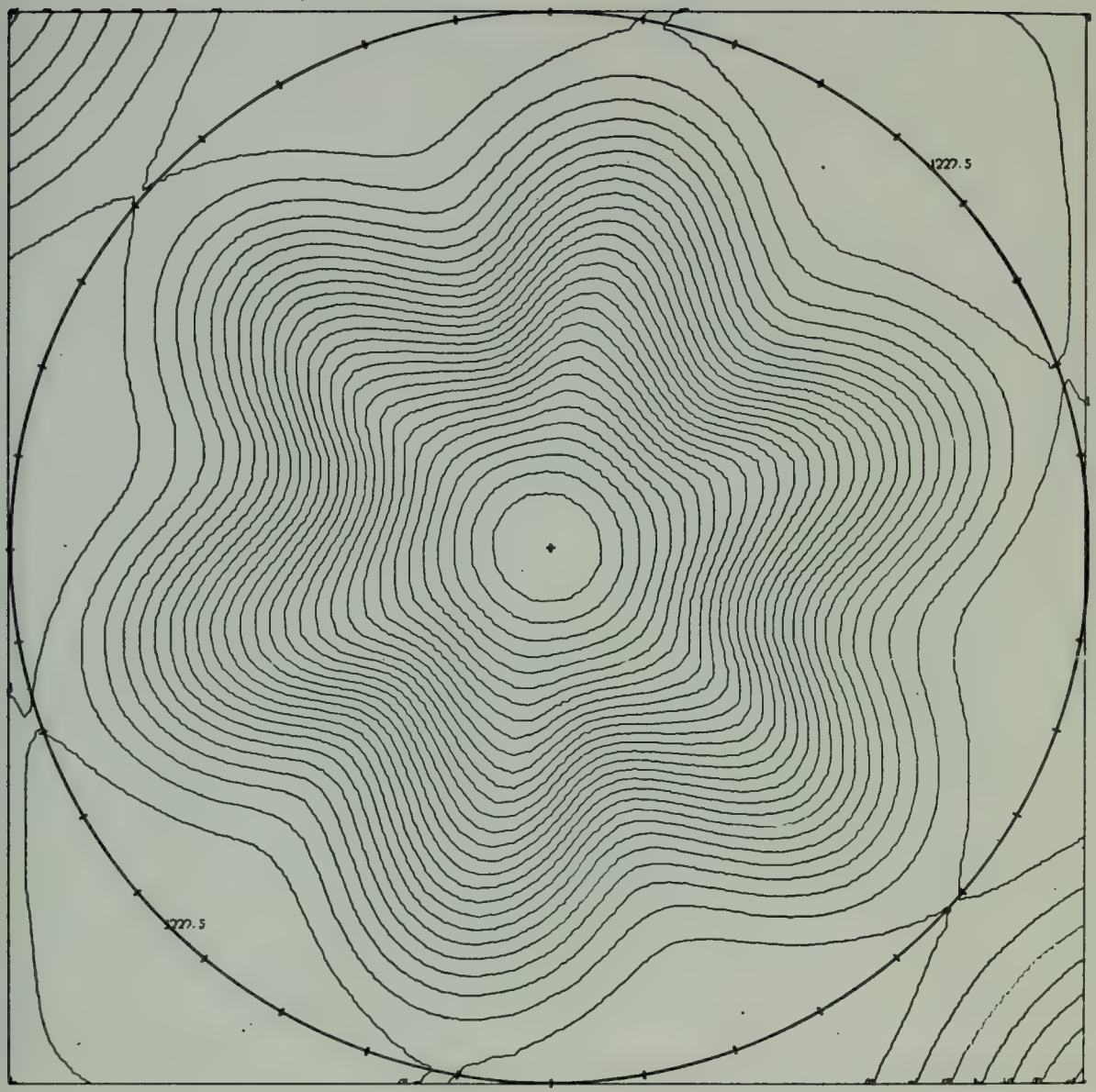

Chart B. 48-hour surface pressure forecast second order differencing, wave number 6, phase speed 12°/day, A = 1000.

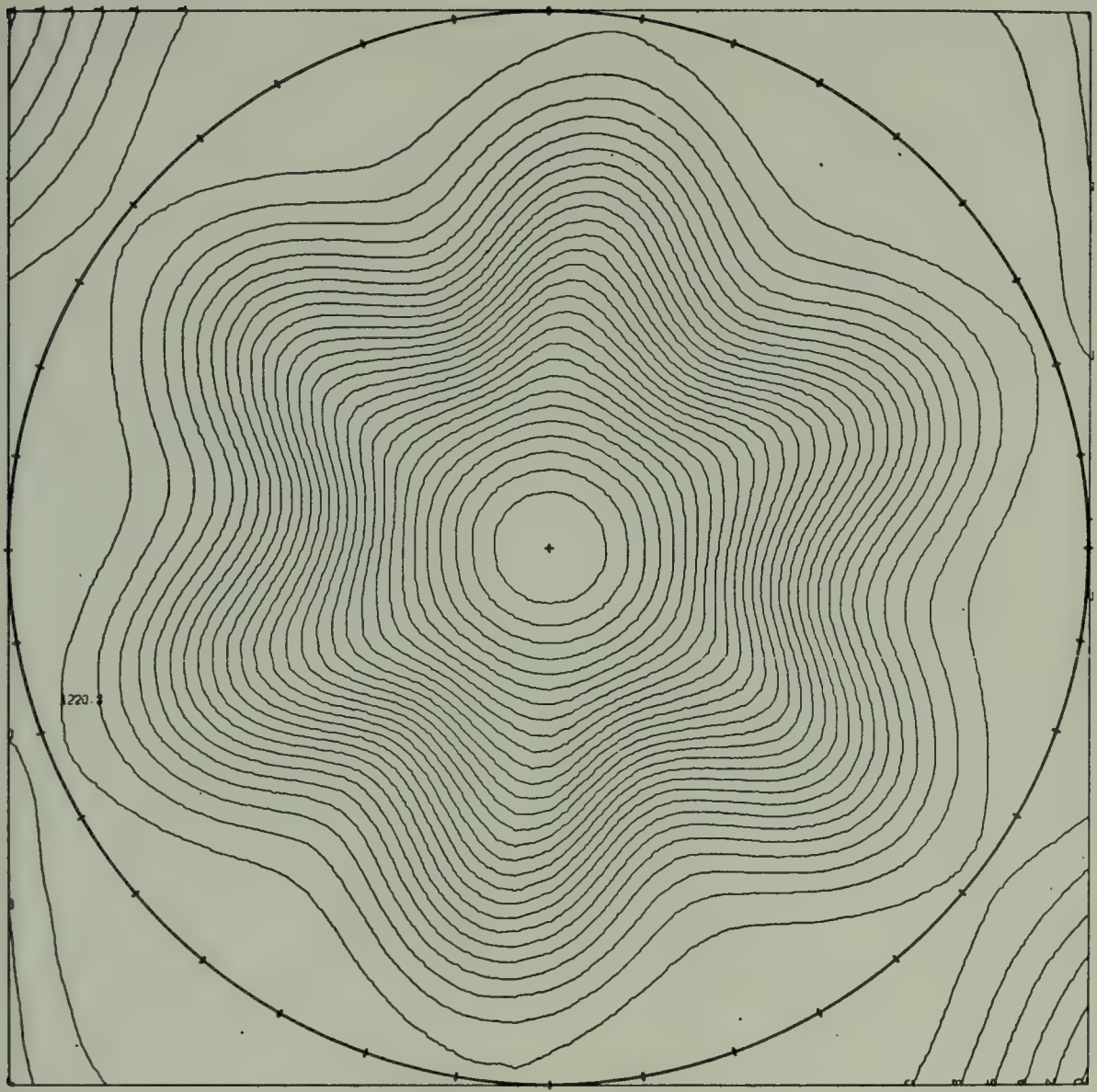

Chart C. 48-hour surface pressure forecast, mixed second and fourth order differencing, wave number 6, phase speed 12°/day, A = 1000.

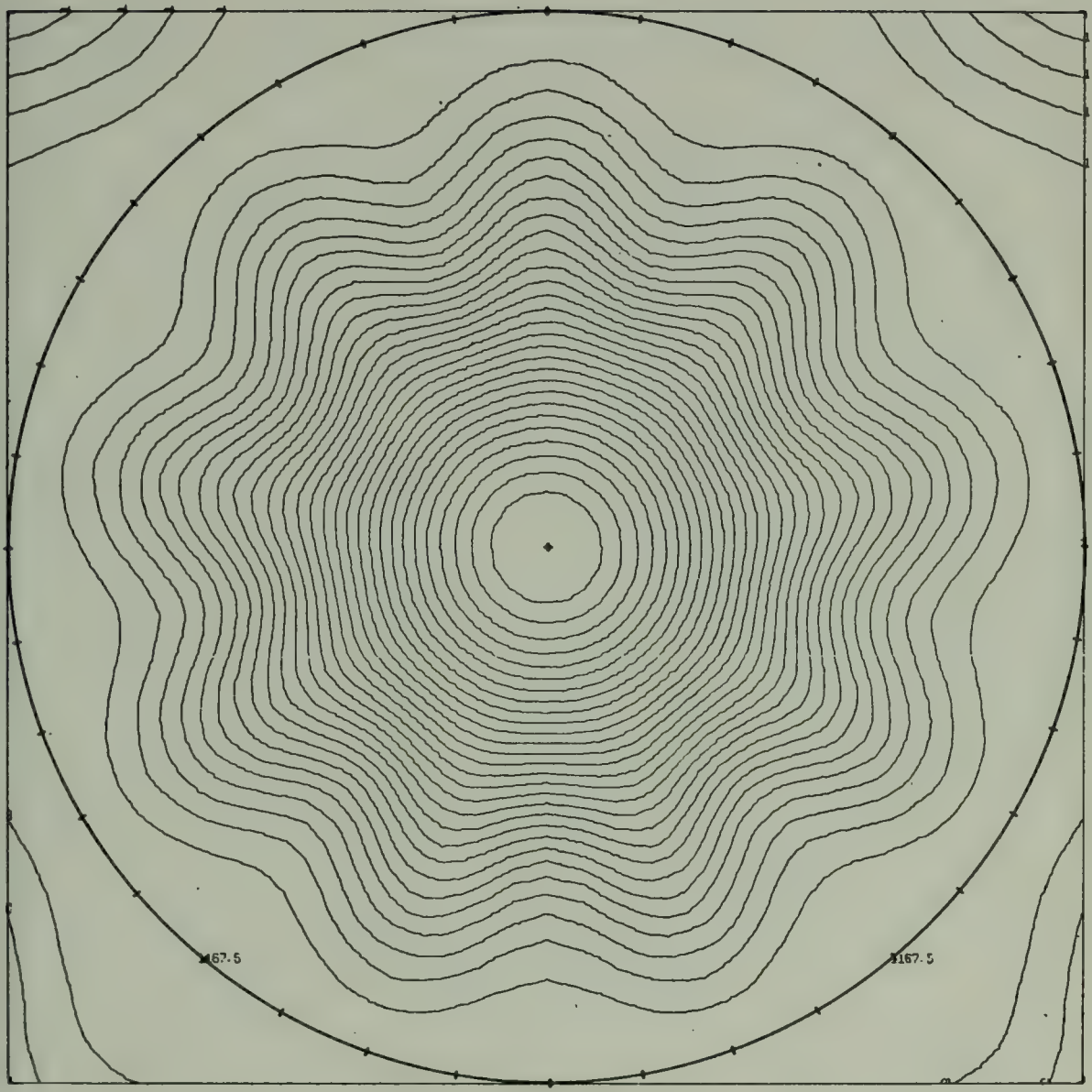

Chart D. Initial surface pressure analysis, wave number 9, phase speed 12°/day, A = 0.1.

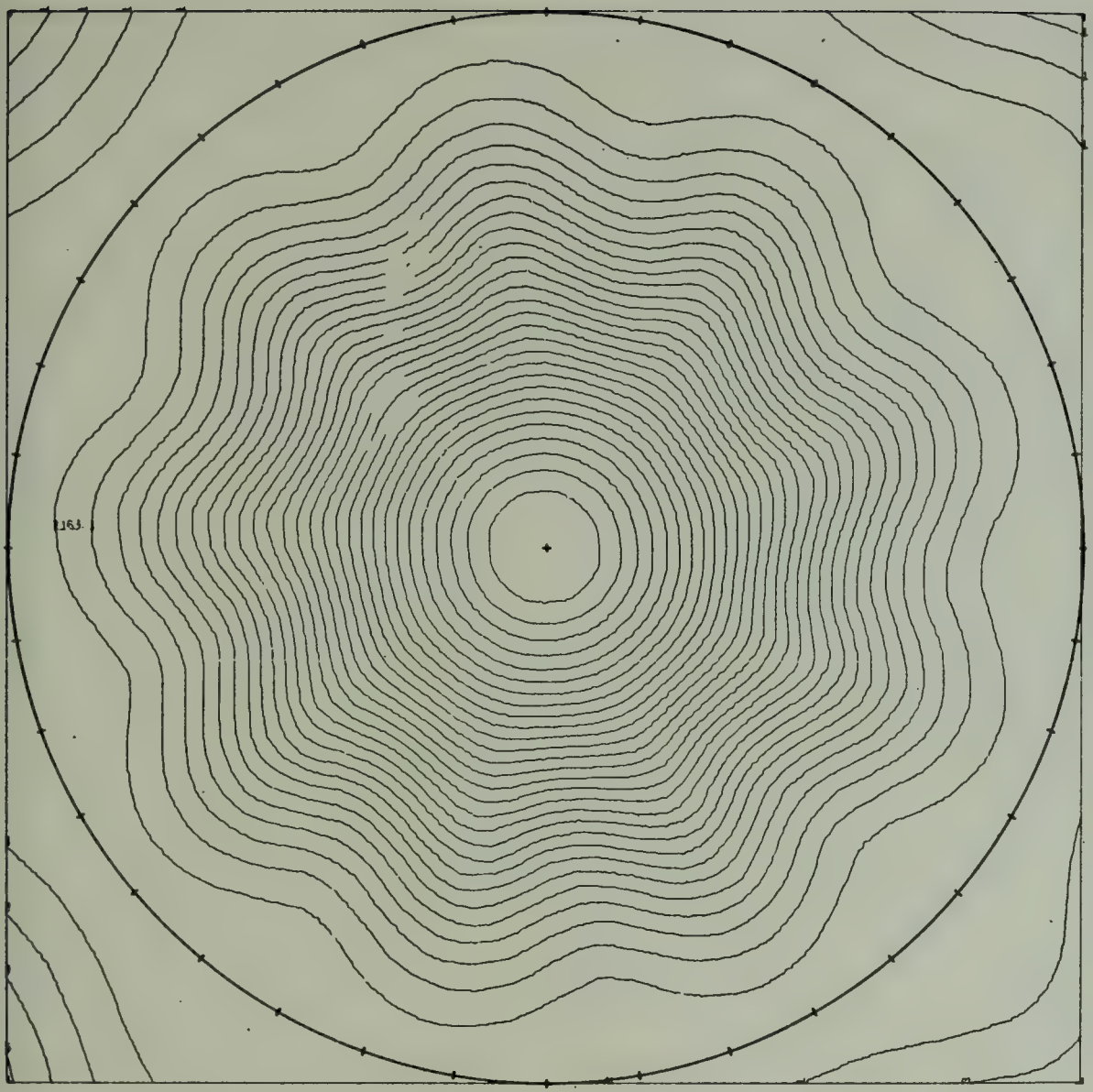

Chart E. 48-hour surface pressure forecast, second order differencing, wave number 9, phase speed 12°/day, A = 0.1.

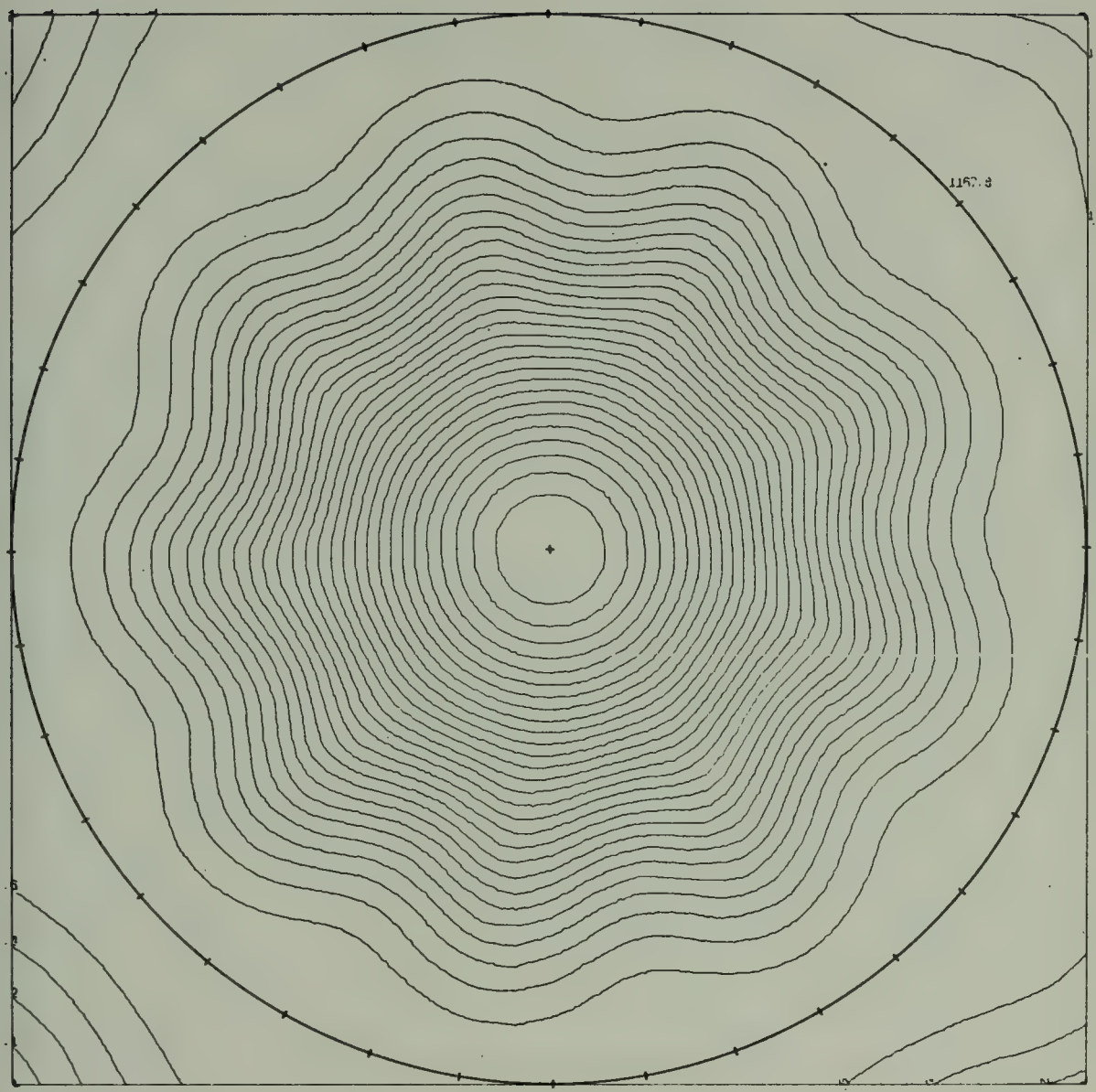

Chart F. 48-hour surface pressure forecast, mixed second and fourth order differencing, wave number 9, phase speed 12°/day, A = 0.1.

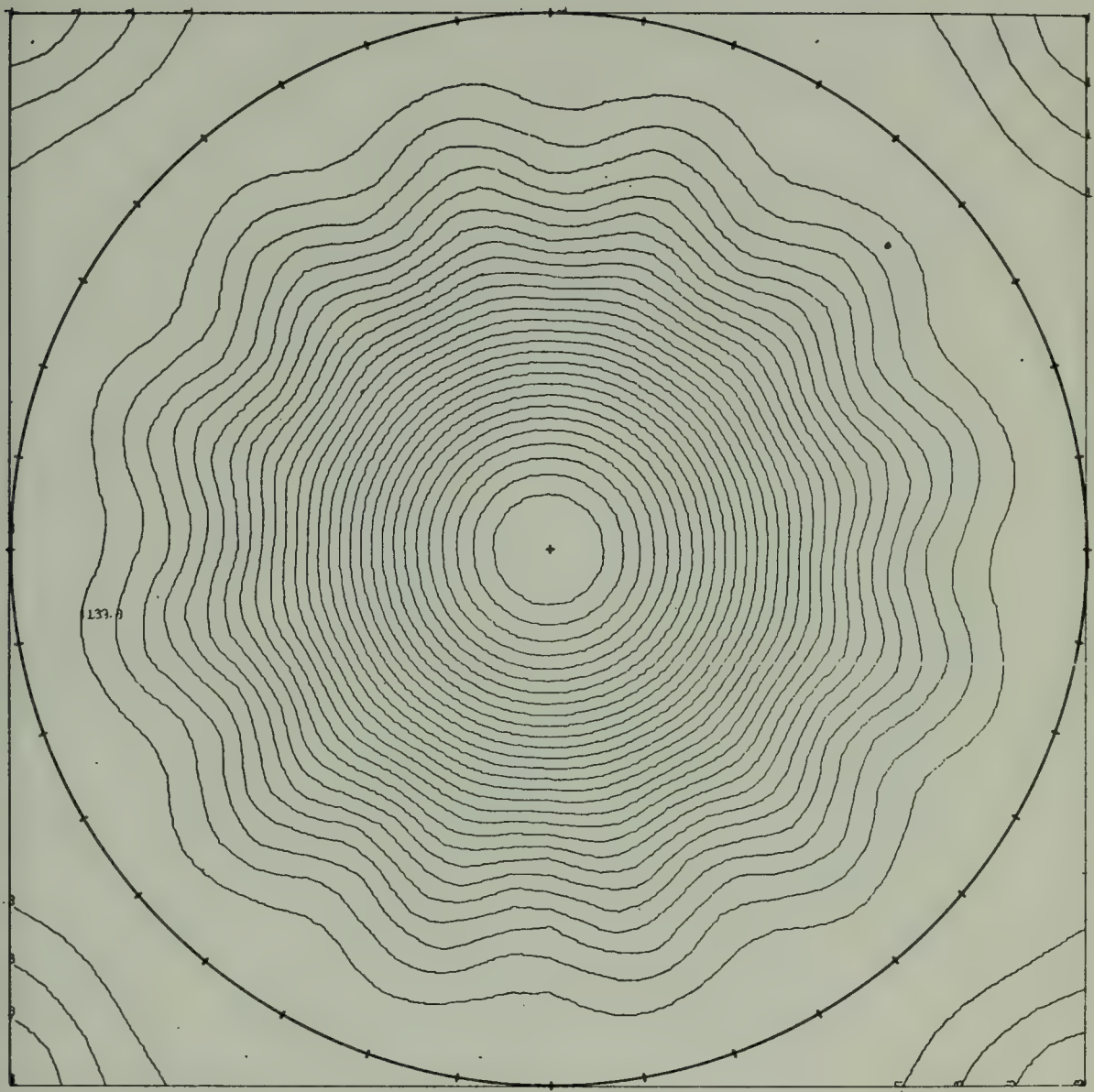

Chart G. Initial surface pressure analysis, wave number 12, phase speed 12°/day, $A = 5.0 \times 10^{-6}$.

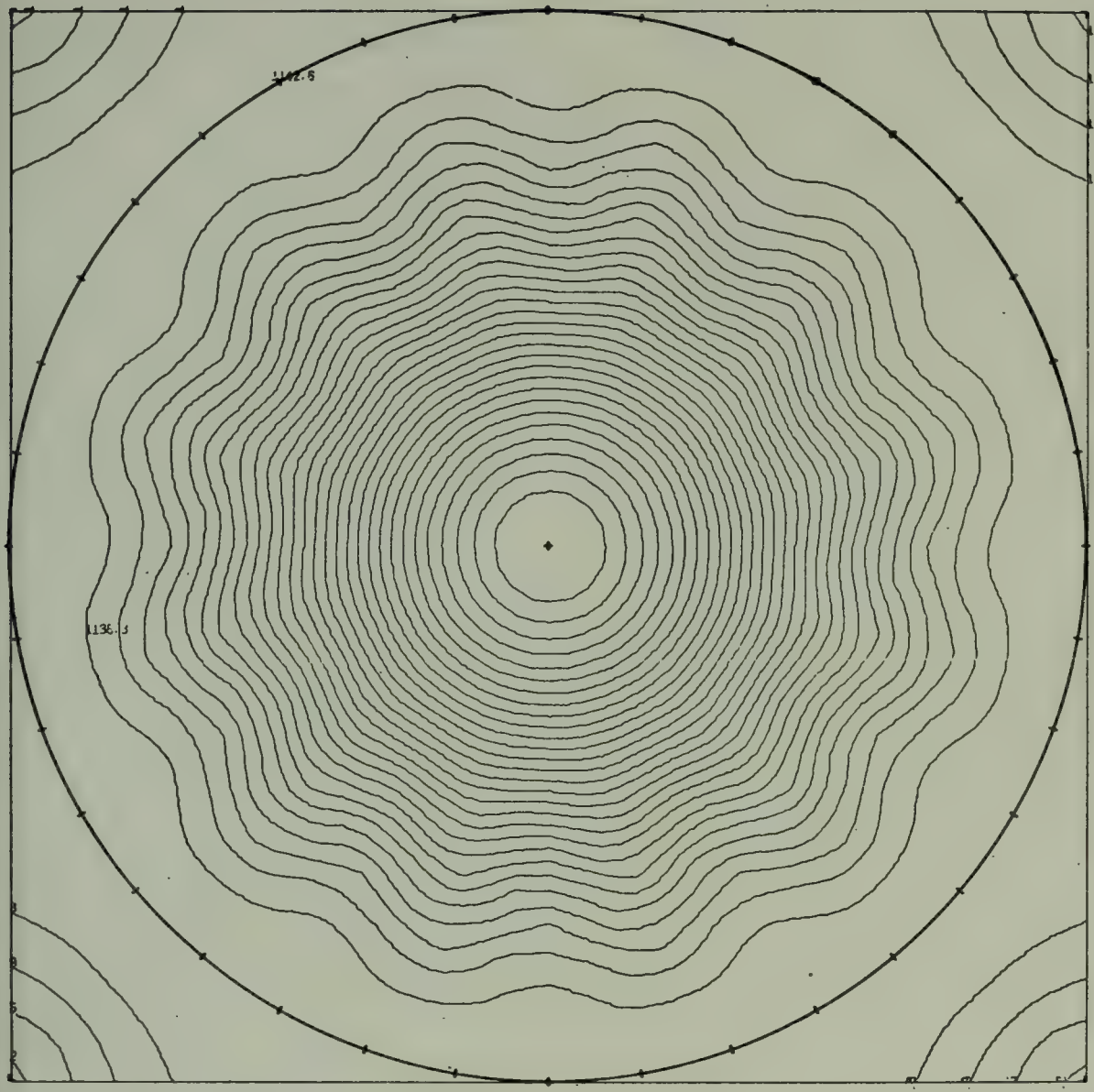

Chart H. 48-hour surface pressure forecast, second order differencing, wave number 12, phase speed 12°/day, $A = 5.0 \times 10^{-6}$.

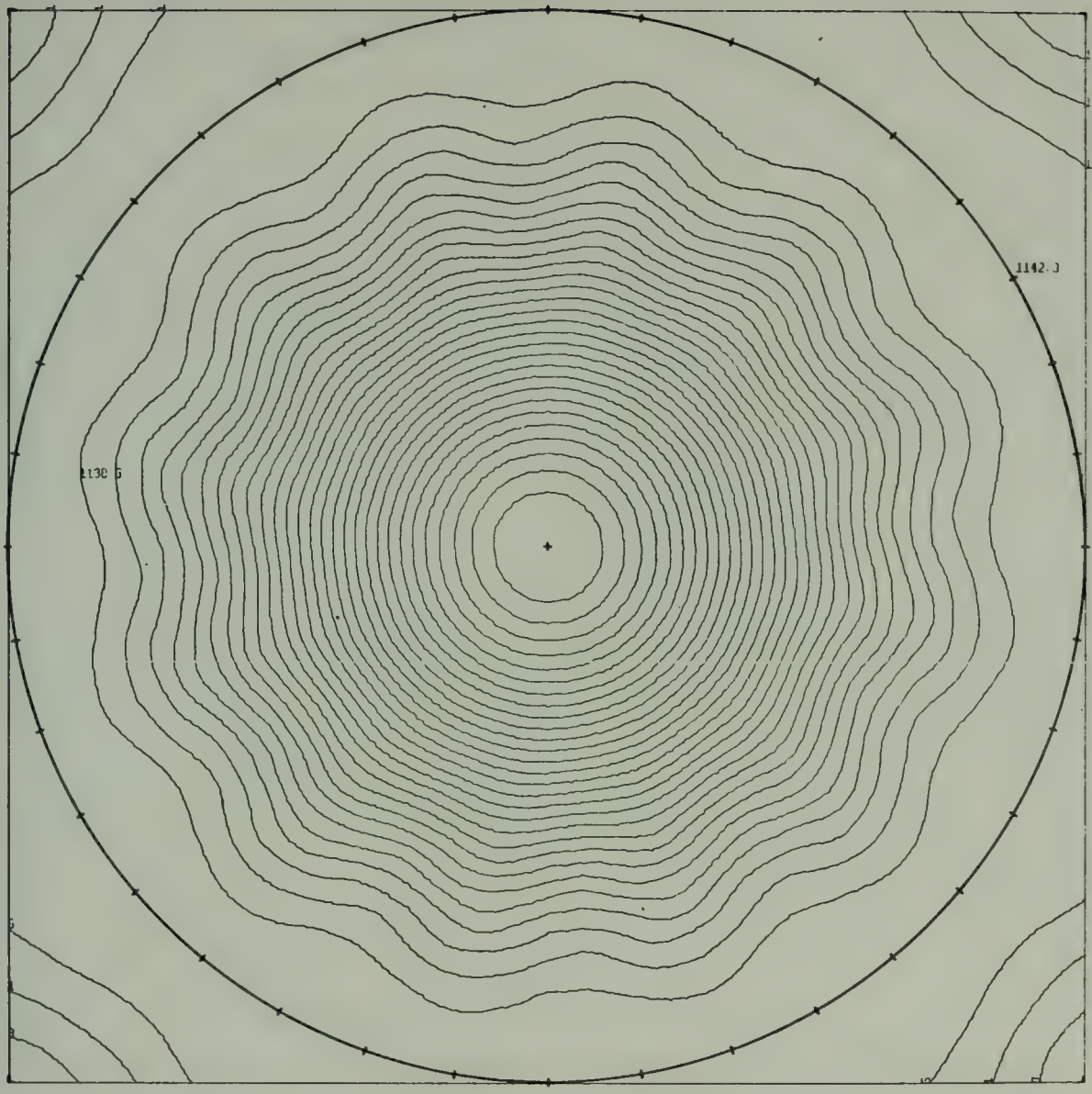

Chart I. 48-hour surface pressure forecast, mixed second and fourth order differencing, wave number 12, phase speed 12°/day, $A = 5.0 \times 10^{-6}$.

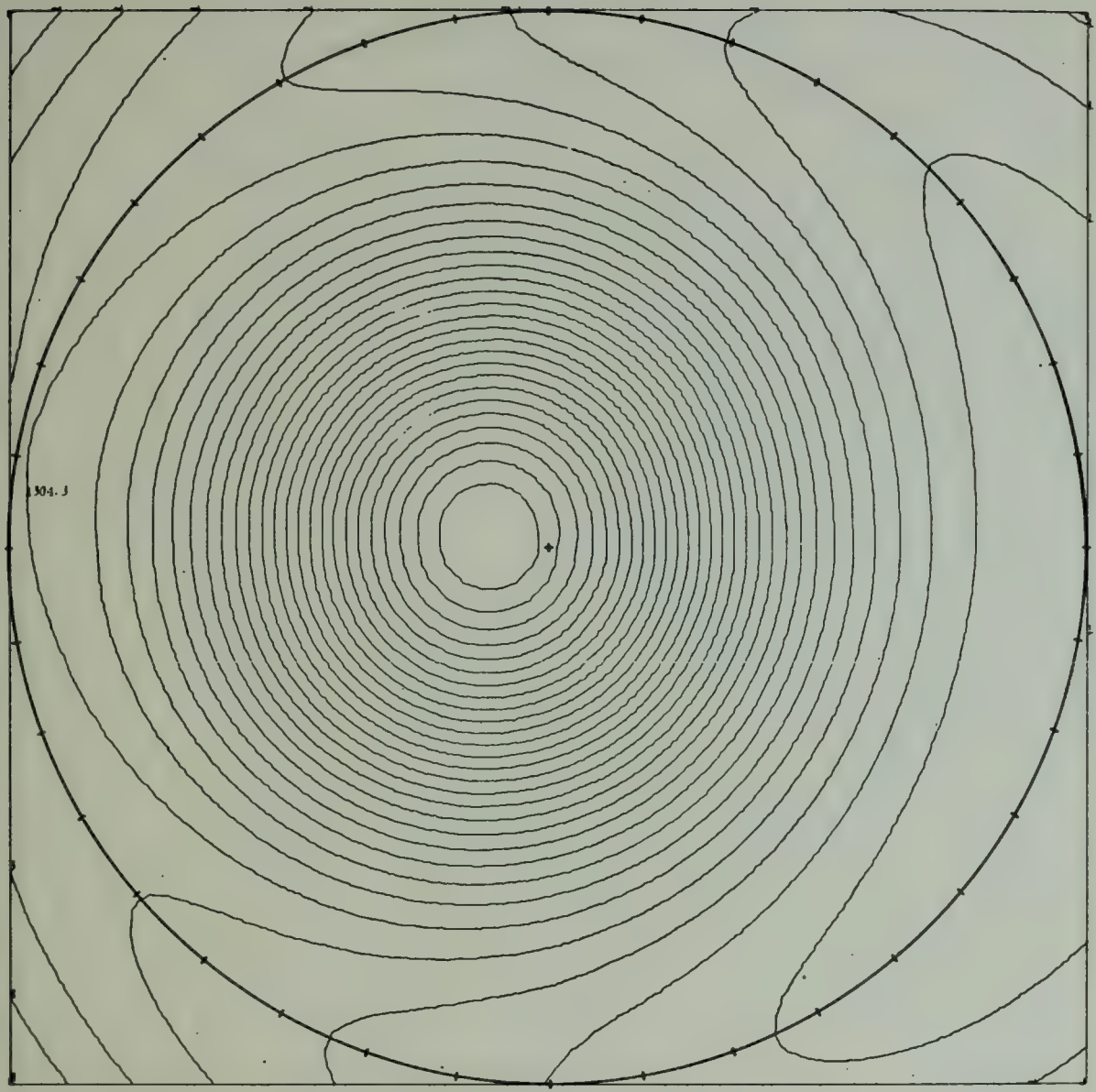

Chart J. Initial surface pressure analysis, wave number 1, phase speed -94.4°/day, A = 3.0×10^7 .

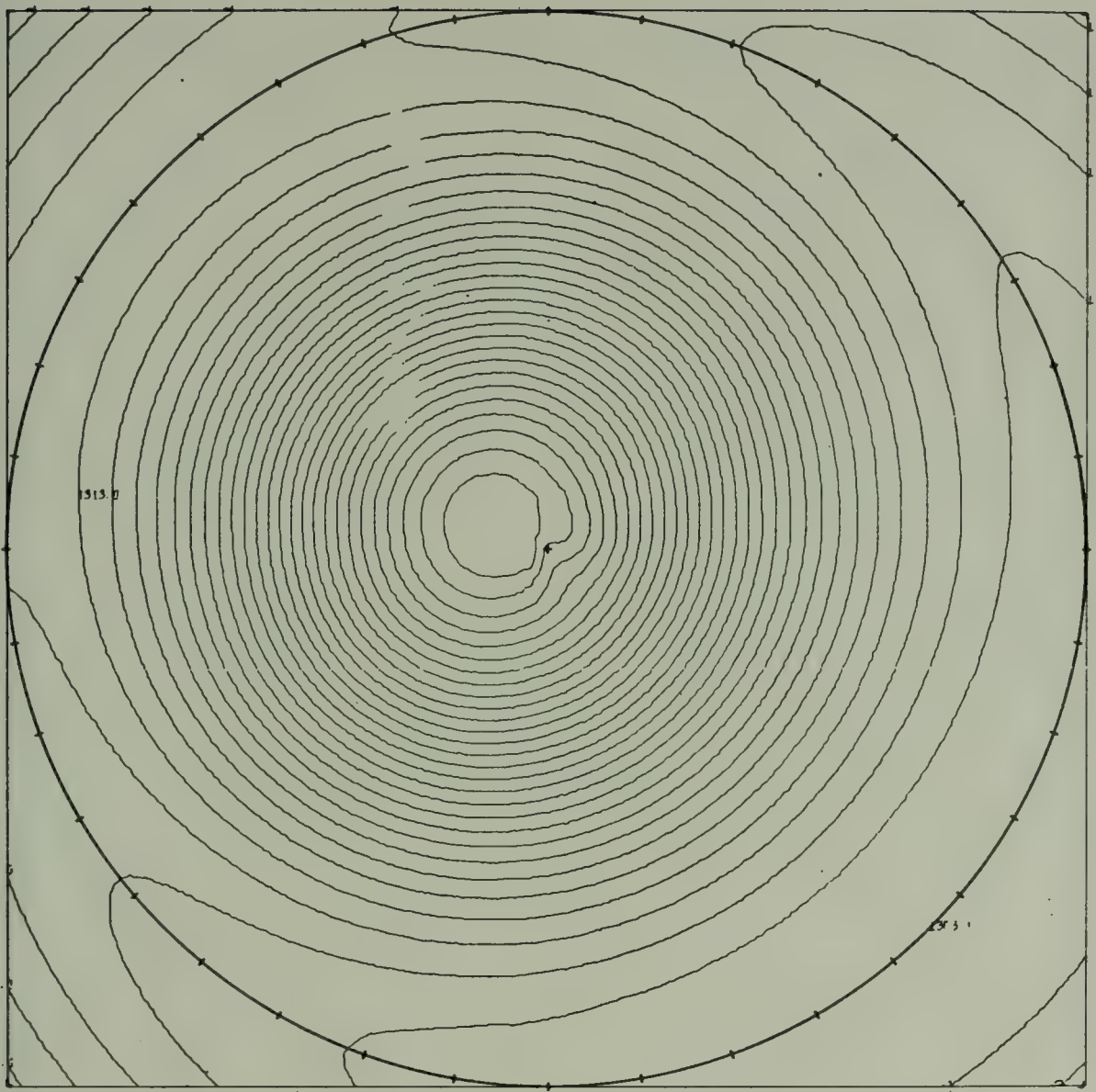

Chart K. 12-hour surface pressure forecast, wave number 1, phase speed -94.4°/day, $A = 3.0 \times 10^7$.

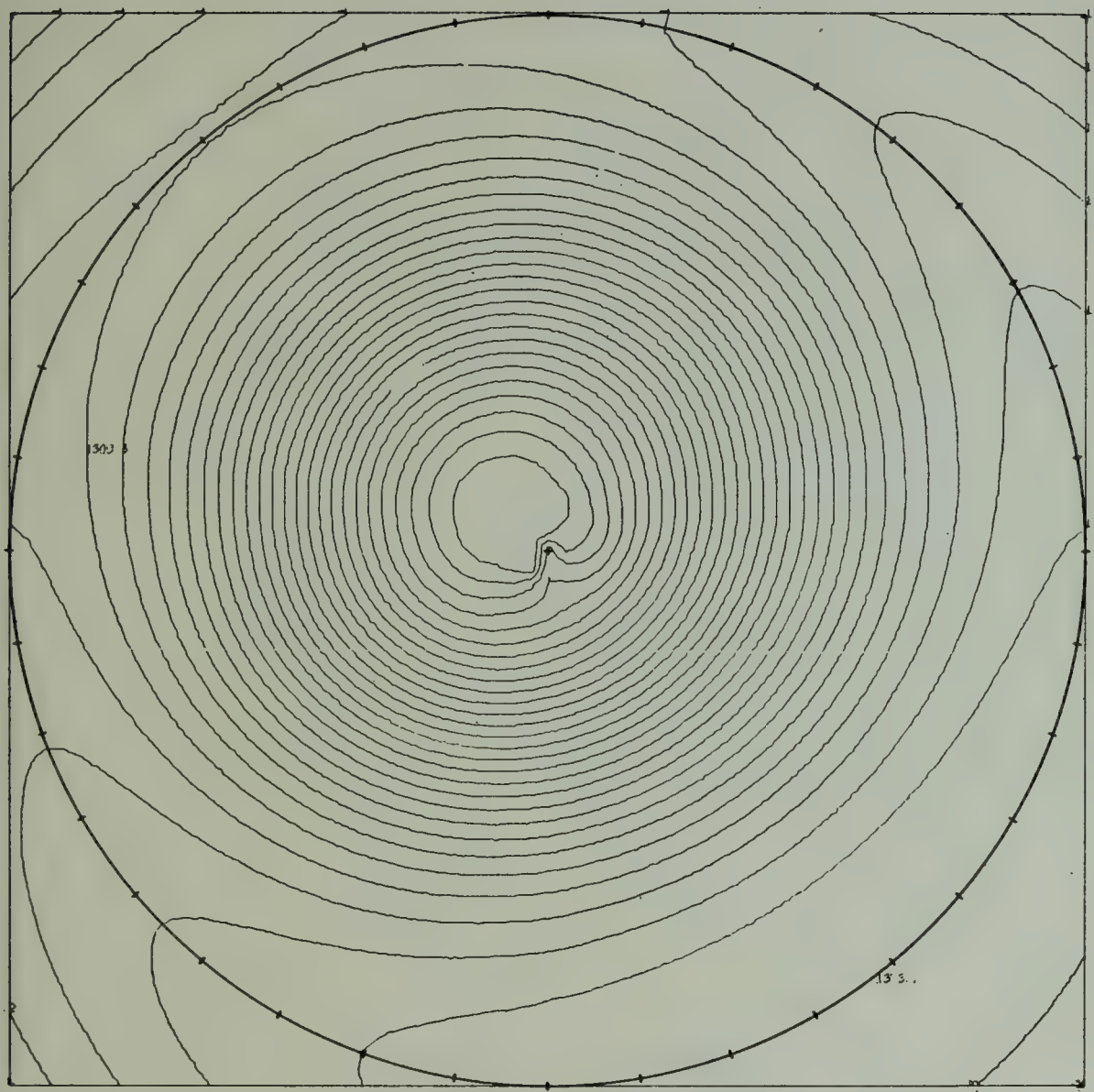

Chart L. 24-hour surface pressure forecast, wave number 1, phase speed -94.4°/day, A = 3.0×10^7 .

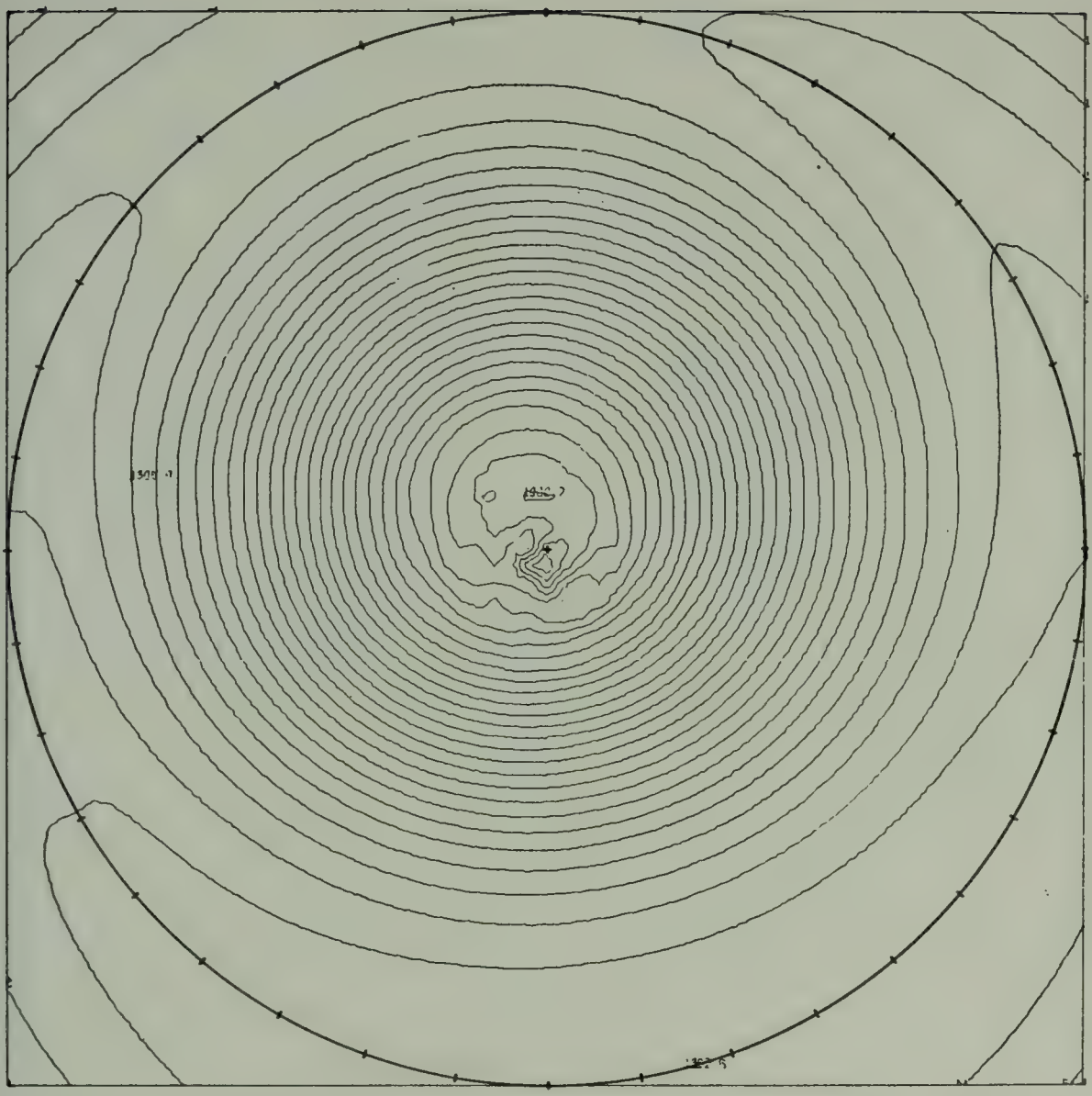

Chart M. 36-hour surface pressure forecast, wave number 1, phase speed -94.4°/day, A = 3.0×10^7 .

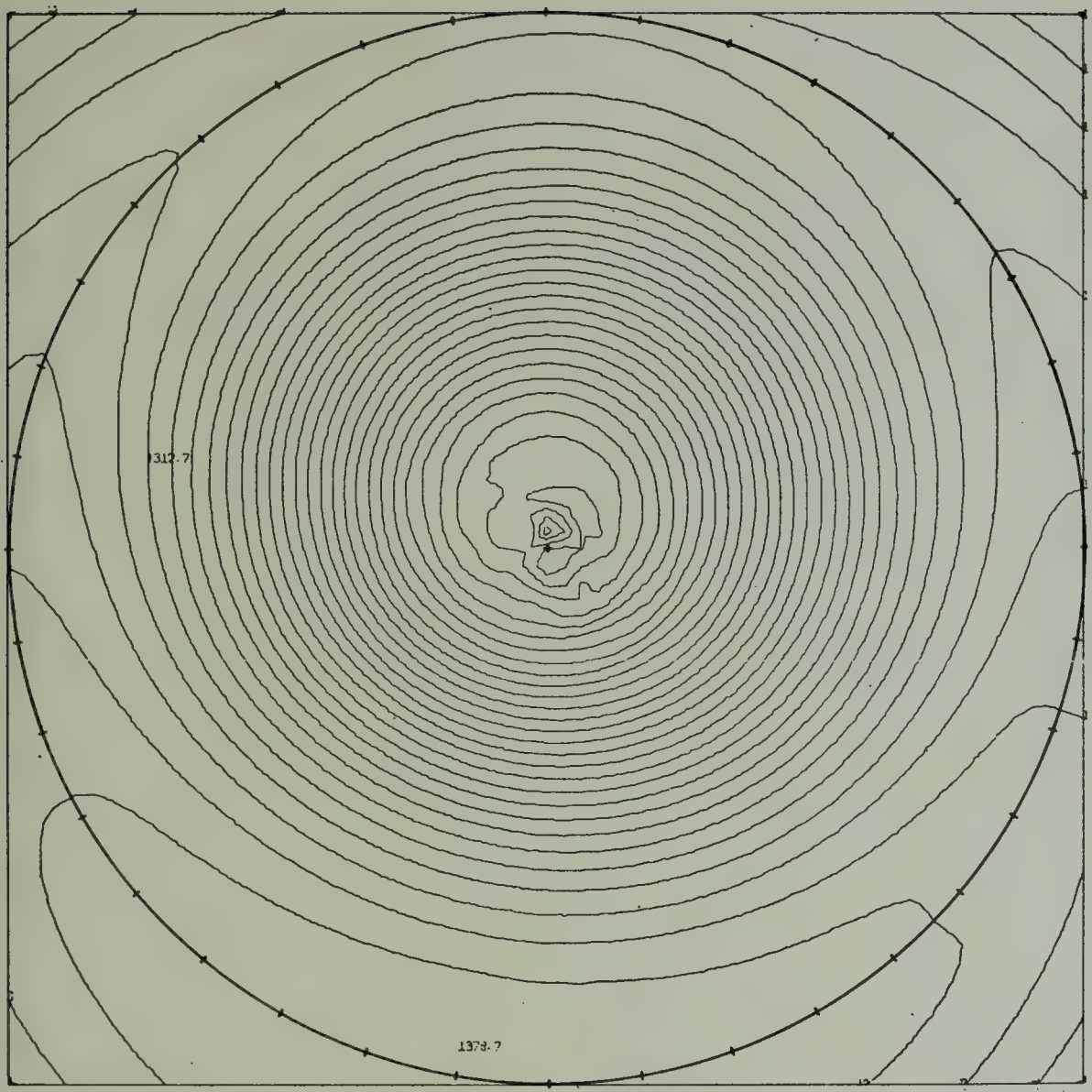

Chart N. 48-hour surface pressure forecast, wave number 1, phase speed -94.4°/day, A = 3.0×10^7 .

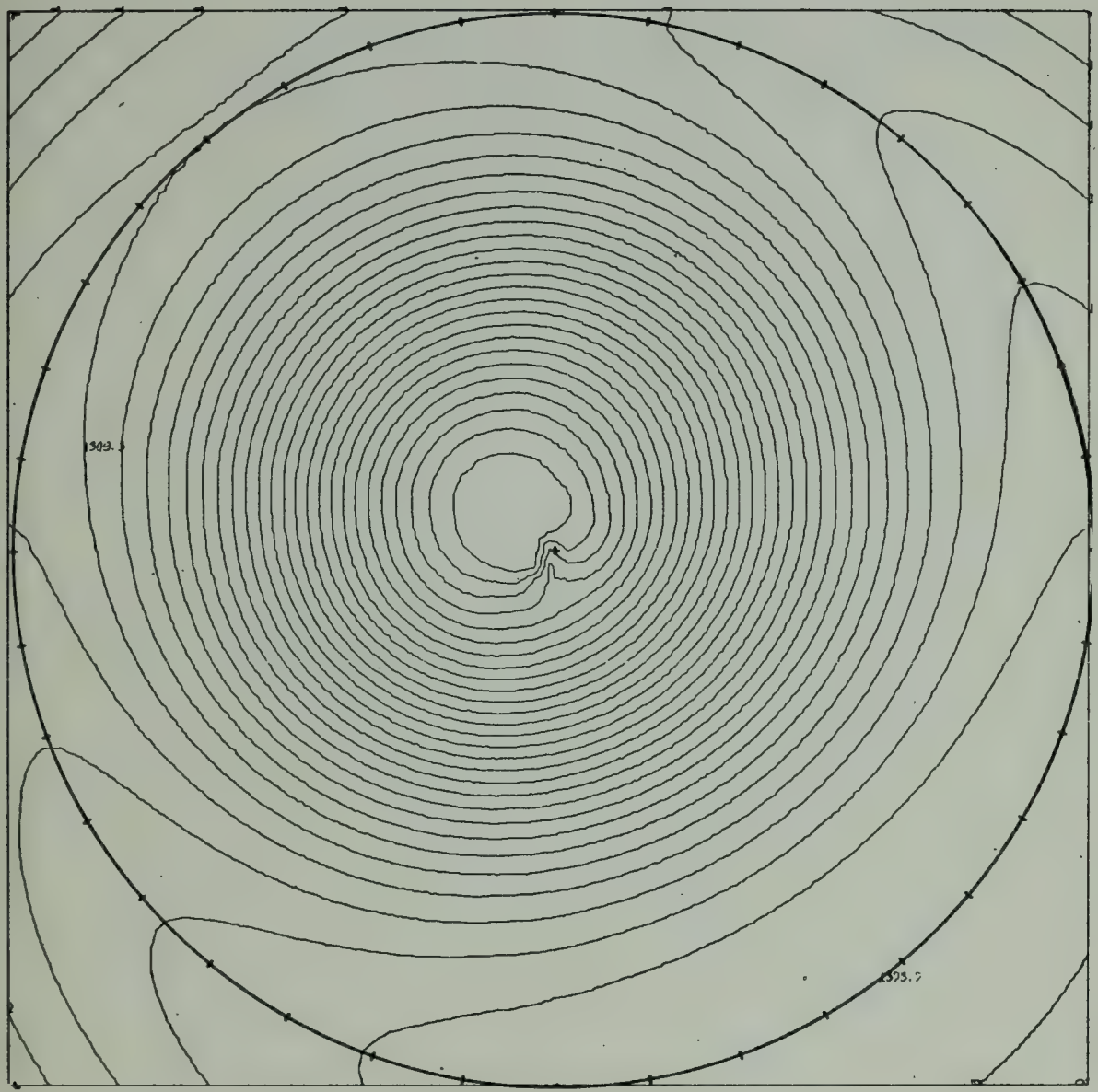

Chart 0. 24-hour surface pressure forecast, wave number 1, phase speed -94.4°/day, A - 3.0×10^7; Arakawa smoothing coefficient squared.

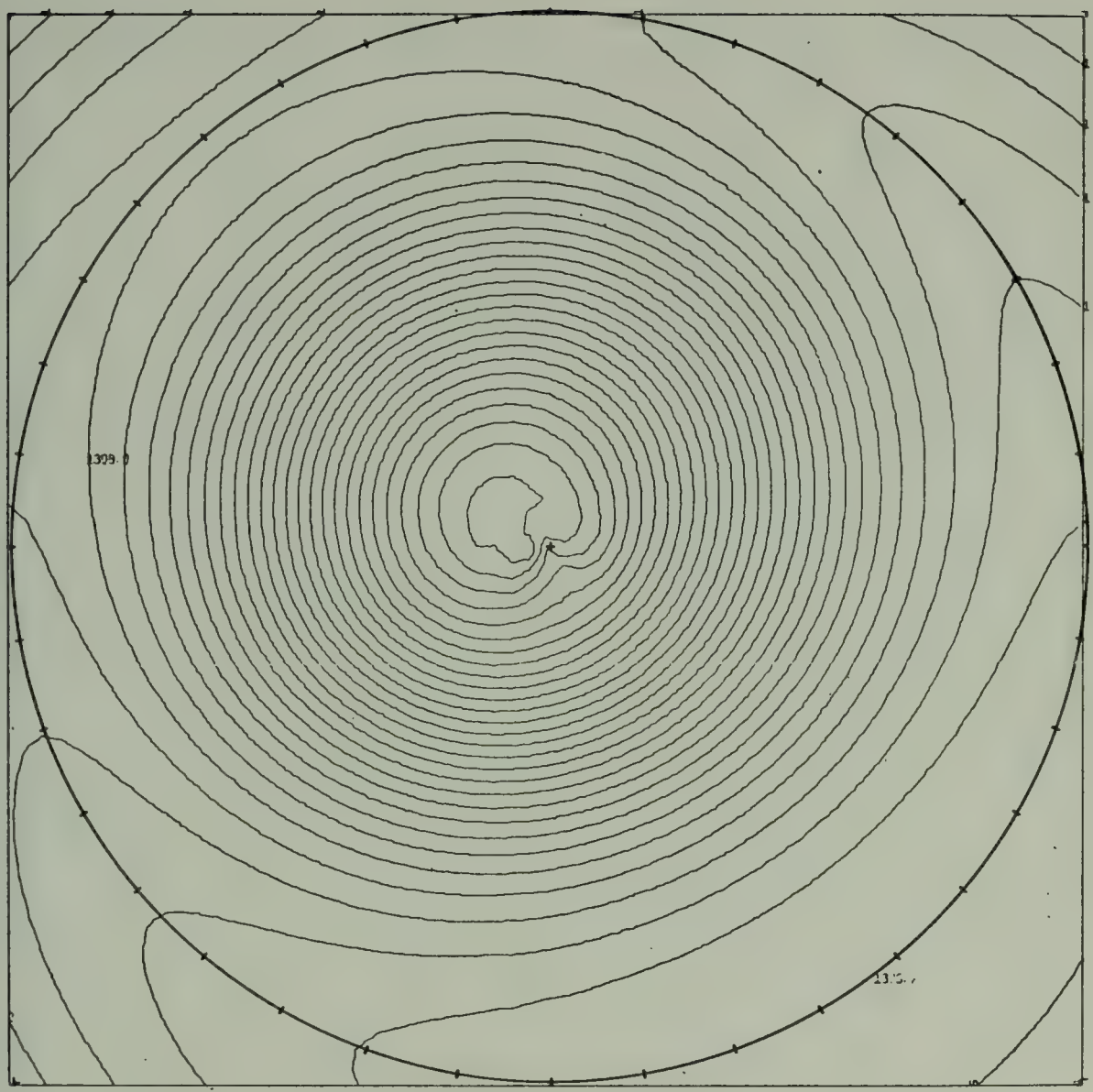

Chart P. 24-hour surface pressure forecast, wave number 1, phase speed -94.4°/day, A = 3.0×10^7; Arakawa smoothing applied to main variables at 3-hour intervals.

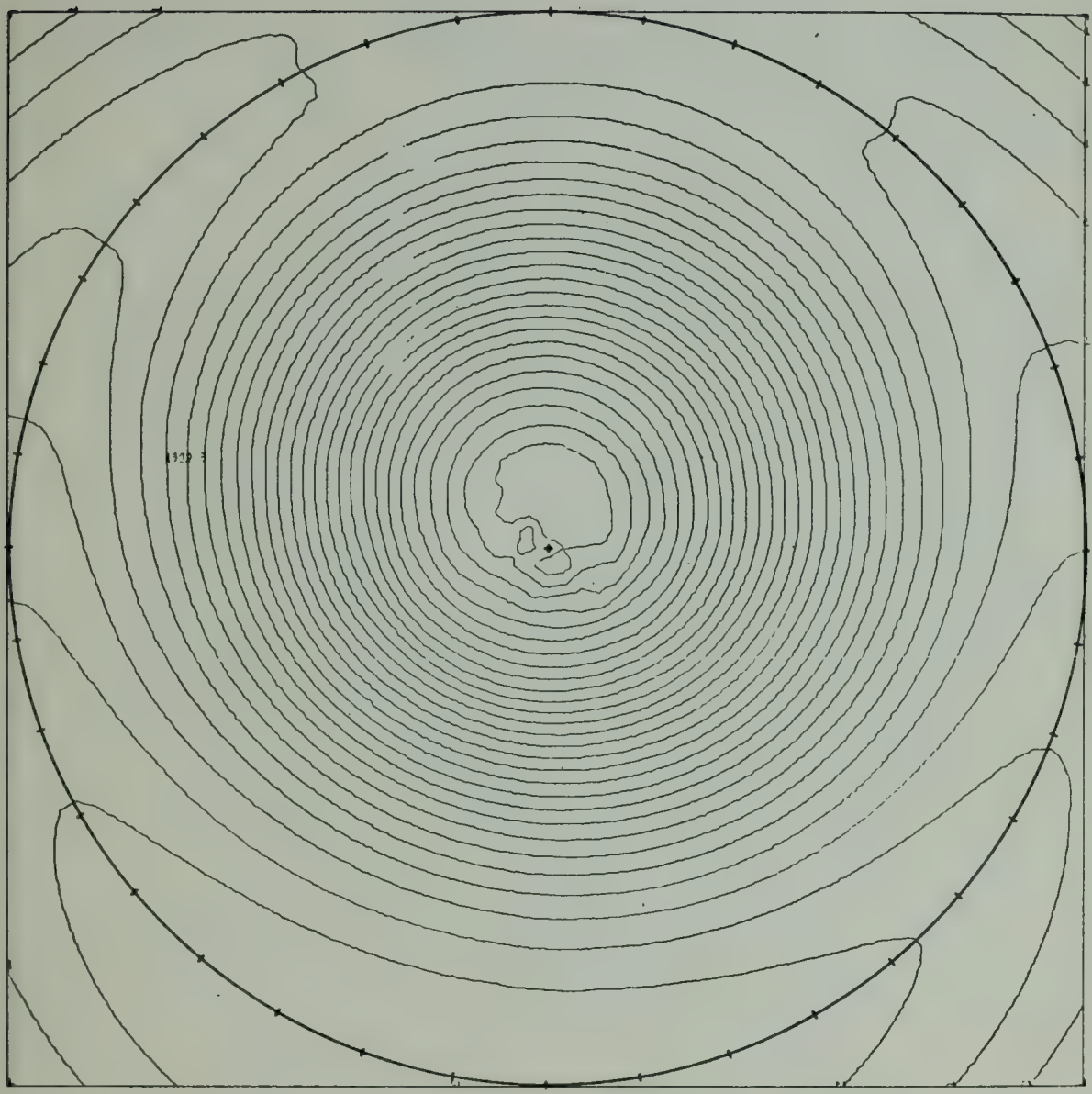

Chart Q. 48-hour surface pressure forecast, wave number 1, phase speed -94.4°/day, A = 3.0×10^7, Arakawa smoothing applied to main variables at 3-hour intervals.

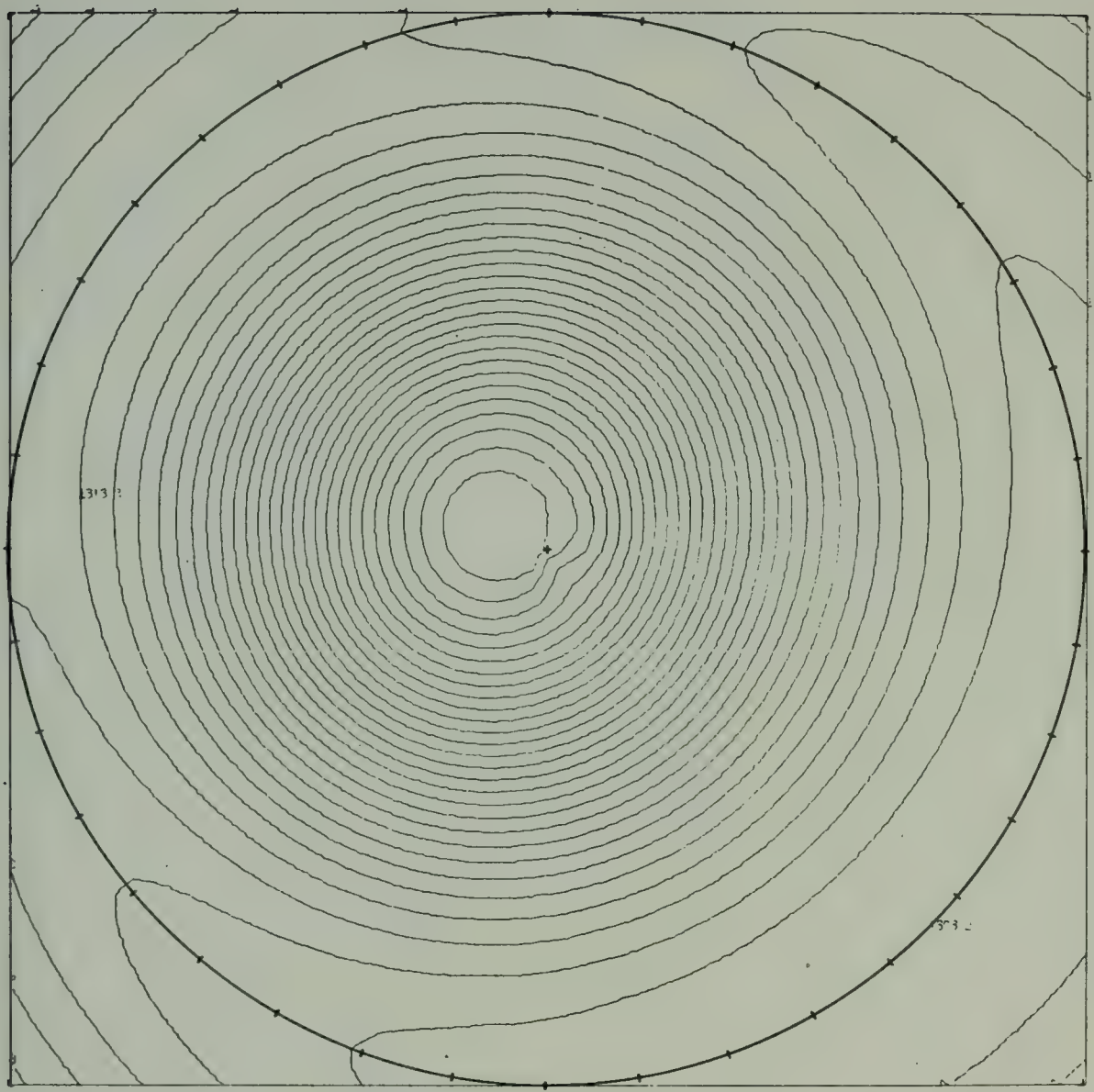

Chart R. 12-hour surface pressure forecast, wave number 1, phase speed -94.4°/day, A = 3.0×10^7, modified output interpolation scheme.

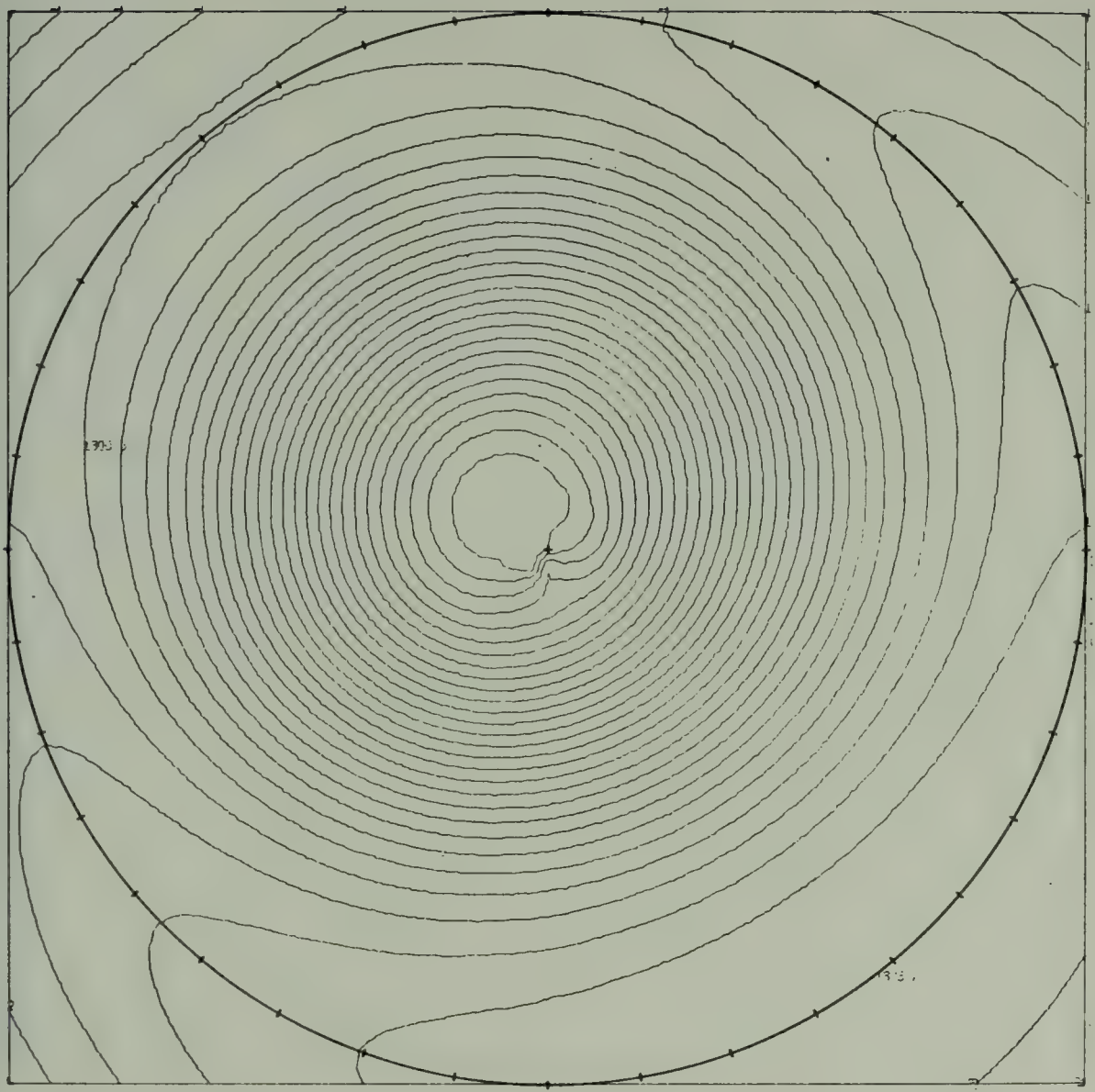

Chart S. 24-hour surface pressure forecast, wave number 1, phase speed -94.4°/day, A = 3.0×10^7, modified output interpolation scheme.

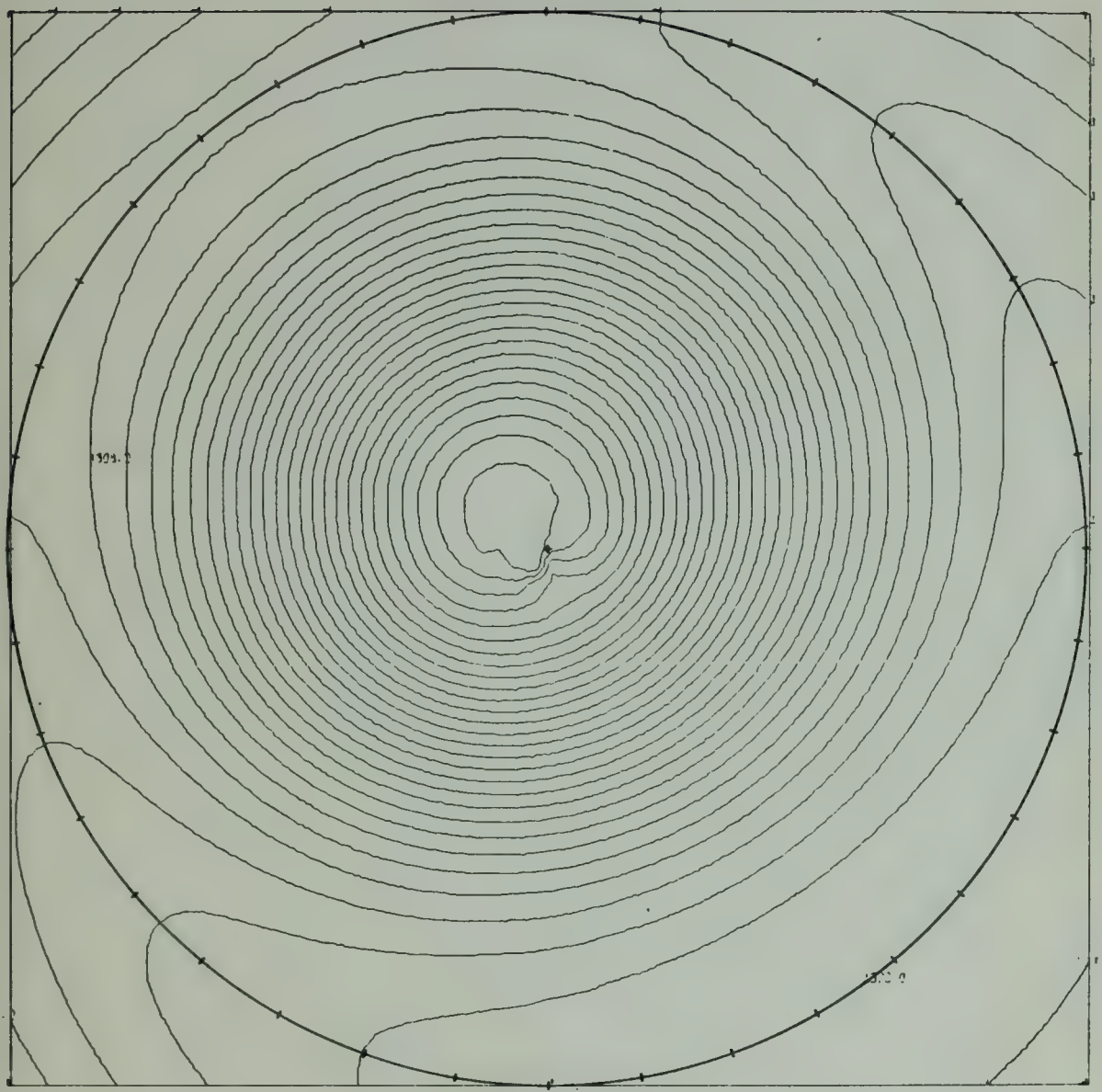

Chart T. 24-hour surface pressure forecast, wave number 1, phase speed -94.4°/day, $A = 3.0 \times 10^7$, modified output interpolation scheme, averages used for polar values.

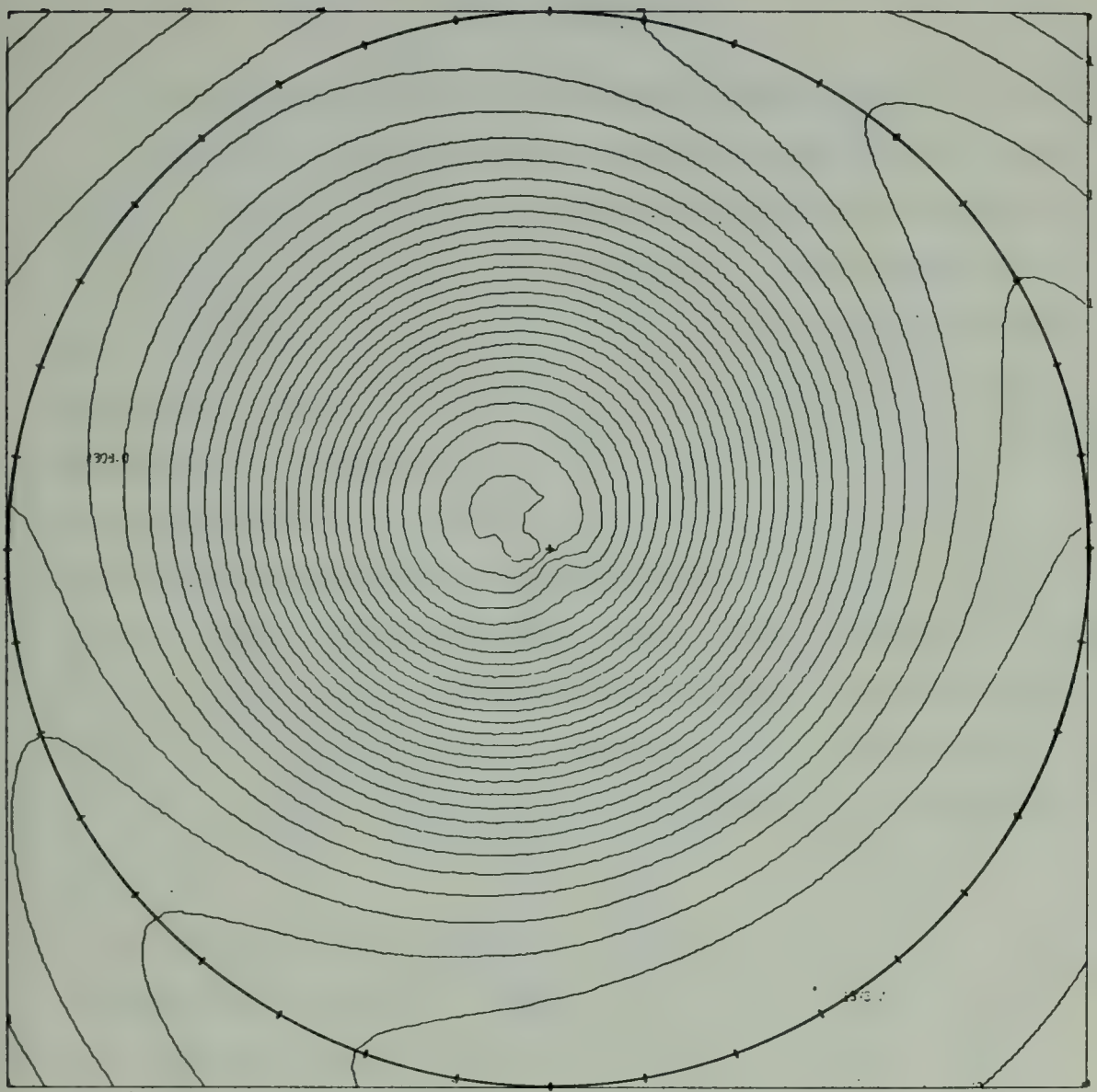

Chart U. 24-hour surface pressure forecast, wave number 1, phase speed -94.4°/day, A = 3.0×10^7, modified output interpolation scheme, Arakawa smoothing applied to main variables at 3-hour intervals.

V. CONCLUSIONS

The experiments comparing second order differencing and the mixed second and fourth order differencing scheme indicate that in general the mixed differencing scheme provides a much closer approximation to the true phase speed. Phase speeds using second order differencing tended to decrease and therefore become more inaccurate with increasing latitude. The mixed differencing scheme produced phase speeds which tended to increase with latitude therefore becoming more accurate. As the wavelength of the harmonic waves became shorter the mixed differencing scheme gave increasingly better phase speeds in comparison with the second order phase speeds. This is especially evident in Experiment III where wave number 12 was used. It should be noted however that both schemes when compared only with themselves on the basis of wave number became steadily less accurate as the wave number increased.

The distortion in the cross-polar flow was in part due to the interpolation scheme which transformed the spherical grid to a 63 x 63 polar stereographic grid. A great deal of the remaining "noise" at the pole can be removed by applying Arakawa smoothing at three-hour intervals to the main variables.

The application of Arakawa smoothing on a polar stereographic plane projection for the main vector variables caused the model to become unstable. Squaring the Arakawa smoothing coefficient did not have a beneficial effect on the cross-polar flow. Application of the Arakawa

smoothing technique to the main variables at every time step smoothed the cross-polar flow somewhat but was not as effective as the three-hour application. The use of 85° latitude averages for the polar quantities led to a small improvement in the forecast.

APPENDIX A

FINITE DIFFERENCE EQUATIONS

The finite difference equations given here are basically the same as those given in Mihok (1974). Additions have been made to include special handling of the equations near the pole and the discussion of the determination of the gradient of terrain pressure has been changed. Friction, diffusion, and heating and moisture source terms are not included. In the following equations Δt is the time increment, $\Delta\lambda$ is a five degree longitudinal grid increment and $\Delta\theta$ is a 5 degree latitudinal grid increment, and $\Delta\sigma = 0.2$ is the vertical increment between layers. Refer to Figure 1 for the staggered spherical grid arrangement and subscripting. Figure 2 illustrates the vertical grid. It should be noted that in the following difference equations the k subscript on w indicates even sigma levels (0.8, 0.6, 0.4, 0.2) and for all other quantities indicates odd sigma levels (0.9, 0.7, 0.5, 0.3, 0.1).

Longitudinal momentum equation

1. Left hand side

$$\frac{\partial u\pi}{\partial t} \equiv \frac{(\bar{\pi}u)^{n+1}_{ijk} - (\bar{\pi}u)^{n-1}_{ijk}}{2\Delta t} \qquad (1)$$

where

$$\bar{\pi} = \frac{1}{4}(\pi_{ijk} + \pi_{i-1,jk} + \pi_{L,j+1,k} + \pi_{L,j-1,k}) \qquad (1.1)$$

In the above Equation (1.1) the subscript

$$L = i \quad (i \text{ even})$$

$$L = i-1 \quad (j \text{ odd})$$

2. Right hand side

a. Term one

$$-\frac{1}{a\cos\theta}\left[\frac{\partial(uu\pi)}{\partial\lambda}+\frac{\partial(uv\pi\cos\theta)}{\partial\theta}\right]\equiv$$

$$-\frac{1}{a\cos\theta_j}\left[\frac{(u_{ijk}+u_{i+1,j,k})\,\overline{u\bar{\pi}}_{i+1/2,j,k}-(u_{ijk}+u_{i-1,j,k})\,\overline{u\bar{\pi}}_{i-1/2,j,k}}{2\cdot 2\Delta\lambda}\right.$$

$$\left.+\frac{(u_{ijk}+u_{i,j+2,k})\,\overline{v\bar{\pi}}_{i,j-1,k}\cos\theta_{j+1}-(u_{ijk}+u_{i,j-2,k})\overline{v\bar{\pi}}_{i,j-1,k}\cos\theta_{j-1}}{2\cdot 2\Delta\theta}\right] \qquad (2)$$

where $\bar{\pi}$ is computed as in (1.1) and

$$\overline{u\bar{\pi}}_{i+1/2,j,k}\equiv\frac{1}{4}[(u\bar{\pi})_{ijk}+(u\bar{\pi})_{i+1,j,k}+(u\bar{\pi})_{L,j+1,j}+(u\bar{\pi})_{L,j-1,k}] \qquad (2.1)$$

$\overline{u\bar{\pi}}_{i-1/2,j,k}$ is obtained from (2.1) by incremental subscripting.

$$\overline{v\bar{\pi}}_{i,j+1,k}\equiv\frac{1}{4}[(v\bar{\pi})_{ijk}+(v\bar{\pi})_{i,j+2,k}+(v\bar{\pi})_{L,j+1,k}+(v\bar{\pi})_{M,j+1,k}] \qquad (2.2)$$

$\overline{v\bar{\pi}}_{i,j-1,k}$ is obtained from (2.2) by incremental subscripting.

The subscripts

L = i (j odd),

L = i+1 (j even),

M = i-1 (j odd), and

M = i (j even).

When computing the above expressions around the 85° and 80° latitude circles any term requiring an undefined polar quantity is ignored. For example

$$\frac{(u_{i+1,j,k} + u_{ijk})}{2} \overline{u\bar{\pi}}_{i+1/2,j,k}$$

is not included in the computation at 85°S since the $\overline{u\bar{\pi}}_{i+1/2,j,k}$ contains the undefined quantity $(u\bar{\pi})_{L,j-1,k}$.

b. Term two

$$\frac{\pi \partial wu}{\partial \sigma} \equiv \bar{\pi}_{ij} \left[\frac{\bar{w}_{ijk}(u_{i,j,k+1} + u_{ijk}) - \bar{w}_{i,j,k-1}(u_{ijk} + u_{i,j,k-1})}{2\Delta\sigma}\right] \quad (3)$$

where the vertical velocity is defined as

$$w_{ijk} = w_{i,j,k-1} - \frac{\Delta\sigma}{\bar{\pi}_{ij}} \left[\left(\frac{\partial \pi}{\partial t}\right)_{ij}\right.$$

$$\left. + \frac{1}{a \cos\theta_j}\left(\frac{(u\bar{\pi})_{i+1,j,k} - (u\bar{\pi})_{ijk}}{2\Delta\lambda} + \frac{(v\bar{\pi})_{i,j+1,k}\cos\theta_{j+1} - (v\bar{\pi})_{i,j-1,k}\cos\theta_{j-1}}{2\Delta\theta}\right)\right] \quad (4)$$

and the local chance in terrain pressure as

$$\left(\frac{\partial \pi}{\partial t}\right)_{ij} \equiv$$

$$- \sum_{k=1}^{5} \frac{\Delta\sigma}{a \cos\theta_j}\left[\frac{(u\bar{\pi})_{i+1,j,k} - (u\bar{\pi})_{ijk}}{2\Delta\lambda} + \frac{(v\bar{\pi})_{i,j+1,k}\cos\theta_{j+1} - (v\bar{\pi})_{i,j-1,k}\cos\theta_{j-1}}{2\Delta\theta}\right] \quad (5)$$

The $\bar{\pi}$ in the above equations is computed as in (1.1). The $\bar{w}$ terms are computed in the same manner as the $\bar{\pi}$ terms.

When computing w and the local change in terrain pressure at the north pole for the thermodynamic and moisture equations the following expressions are used, as discussed in Section II-D-2,

$$w_{pole,k} = w_{pole,k-1} - \frac{\Delta\sigma}{\pi_{pole}} \left[\left(\frac{\partial\pi}{\partial t}\right)_{pole} + \frac{2\Delta\sigma}{a\Delta\theta 36} \sum_{i=1}^{36} (v\bar{\pi})_{i,35,k}\right] \qquad (6)$$

and

$$\left(\frac{\partial\pi}{\partial t}\right) = - \sum_{k=1}^{5} \frac{2\Delta\sigma}{a\Delta\theta 36} \sum_{i=1}^{36} (v\bar{\pi})_{i,35,k} \qquad (7)$$

In order to compute these quantities at the south pole change the sign of $(v\bar{\pi})$ and the subscript j from 35 to 1 .

c. Term three

$$\frac{\pi uv \tan\theta}{a} = \frac{(u\bar{\pi}v)_{ijk} \tan\theta_j}{a} \qquad (8)$$

with $\bar{\pi}$ as in (1.1).

d. Term four

$$\pi vf \equiv f_j (\bar{\pi}v)_{ijk} \qquad (9)$$

with $\bar{\pi}$ as in (1.1).

e. Term five

$$-\frac{1}{a\cos\theta}\left[RT\frac{\partial\pi}{\partial\lambda} + \pi\frac{\partial\phi}{\partial\lambda}\right] \equiv$$

$$-\frac{1}{a\cos\theta_j}\left[R\bar{T}_{ijk}\left(\frac{\partial\pi}{\partial\lambda}\right)^*_{ij} + \bar{\pi}_{ij}\frac{(\phi_{ijk} - \phi_{i-1,j,k})}{2\Delta\lambda}\right] \qquad (10)$$

where $\bar{\pi}$ is obtained from (1.1) and $\bar{T}$ is computed in the same manner.

Based on Equation (10) of Section II-A the longitudinal derivative of terrain height may be expressed

$$\left(\frac{\partial \pi}{\partial \lambda}\right)^{*} = \frac{\bar{\pi}}{R\bar{T}2\Delta\lambda}\left[\Delta\phi_p - \Delta\phi_\sigma\right] \tag{11}$$

In order to obtain $[\Delta\phi_p - \Delta\phi_\sigma]$ we first use the hypsometric equation to form

$$-\Delta\phi_\sigma = R\bar{T}\left[\ell n\, \pi_i - \ell n\, \pi_{i-1}\right] \tag{12}$$

The right hand side of (12) can be modified to

$$-\Delta\phi_\sigma = R\bar{T}[\ell n\pi_i - \ell n\bar{\pi}_i + \ell n\bar{\pi}_i - \ell n\bar{\pi}_{i-1}] \tag{13}$$

without changing the equality.

Bringing $\bar{T}$ inside the parenthesis and computing it in a special way on either side of the velocity point yields

$$[\Delta\phi_p - \Delta\phi_\sigma]_{ijk} =$$

$$R[\bar{T}_{LEFT,k}(\ell n\pi_{ij} - \ell n\bar{\pi}_{ij}) + \bar{T}_{RIGHT}(\ell n\bar{\pi}_{ij} - \ell n\pi_{i-1,j})] \tag{14}$$

$\bar{T}_{LEFT}$ and $\bar{T}_{RIGHT}$ are special mean temperatures derived over the five degree grid distance from the computational velocity point to the adjacent mass point either on the right or on the left. The following method is used to compute these temperatures. The subscript S indicates side (either right or left).

(1) If $(\ell n\bar{\pi}_{ij} - \ell n\pi_S) < 0$ or $k = 1$, (i.e. $\sigma = 0.9$) then

$$\bar{T}_{S,k} = T_{S,k} + \frac{(T_{S,k+1} - T_{S,k})}{2}\,\frac{(\ell n\pi_{ij} - \ell n\bar{\pi}_S)}{(\ell n\sigma_{k+1} - \ell n\sigma_k)} \tag{15}$$

Equation (15) takes care of the situation where the pressure on the sigma surface at the computational point is less than the sigma surface pressure at an adjacent mass point. The mean change of temperature between the layers is multiplied by the logarithmic slope of the sigma surface $\frac{\Delta \ell n \pi}{\Delta \ell n \sigma}$. This is used to modify the temperature of the lower layer. The end result is to interpolate the value of the geopotential at the mass point to the same pressure surface as the computational point before integration takes place.

(2) If $(\ell n \bar{\pi}_{ij} - \ell n \pi_S) > 0$ or $k = 5$, $(\sigma = 0.1)$, then

$$\bar{T}_{S,k} = T_{S,k-1} + \frac{(T_{S,k} - T_{S,k-1})}{2} \left[\frac{(\ell n \bar{\pi}_{ij} - \ell n \pi_S) + (\ell n \sigma_k - \ell n \sigma_{k-1})}{\ell n (\sigma_k - \ell n \sigma_{k-1})}\right] \qquad (16)$$

Equation (16) comes into play when the pressure on the sigma surface at the computational point is less than the pressure on the sigma surface at an adjacent mass point. The mean change of temperature between the layers is multiplied by the logarithmic slope of the pressure surface $\frac{\Delta \ell n \pi \sigma}{\Delta \ell n \sigma}$. This is used to modify the upper layer. The end result is to interpolate the value of the geopotential at the mass point to the same pressure surface as the computational point before integration takes place.

This computational scheme for $\frac{\partial \pi}{\partial \lambda}$ is intended to reduce truncation error when differencing over steep terrain. Even though a flat earth is used in this thesis the terrain pressure spatial derivatives using this scheme were allowed to remain.

Latitudinal momentum equation

1. Left hand side

$$\frac{\partial v\bar{\pi}}{\partial t} \equiv \frac{(\bar{\pi}v)^{n+1}_{ijk} - (\bar{\pi}v)^{n-1}_{ijk}}{2\Delta t} \tag{17}$$

where $\bar{\pi}$ is computed as in (1.1).

2. Right hand side

a. Term one

$$-\frac{1}{a\cos\theta_j}\left[\frac{\partial(\pi vv)}{\partial\lambda} + \frac{\partial(\pi vv\cos\theta)}{\partial\theta}\right] \equiv$$

$$-\frac{1}{a\cos\theta_j}\left[\frac{(v_{ijk}+v_{i+1,j,k})\overline{u\bar{\pi}}_{i+1/2,j,k} - (v_{ijk}+v_{i-1,j,k})\overline{u\bar{\pi}}_{i-1/2,j,k}}{2 \cdot 2\Delta\lambda}\right.$$

$$\left. + \frac{(v_{ijk}+v_{i,j+2,k})\overline{v\bar{\pi}}_{i,j+1,k}\cos\theta_{j+1} - (v_{ijk}+v_{i,j-2,k})\overline{v\bar{\pi}}_{i,j-1,k}\cos\theta_{j-1}}{2 \cdot 2\Delta\theta}\right] \tag{18}$$

where the $\overline{u\bar{\pi}}$ and $\overline{v\bar{\pi}}$ terms are computed as in (2.1) and (2.2).

b. Term two

$$\pi\frac{\partial(wv)}{\partial\sigma} = \bar{\pi}_{ij}\left[\frac{\bar{w}_{ijk}(v_{i,j,k+1}+v_{ijk})}{2\Delta\sigma} - \frac{\bar{w}_{i,j,k-1}(v_{ijk}+v_{i,j,k-1})}{2\Delta\sigma}\right] \tag{19}$$

The $\bar{w}$ and $(\frac{\partial\pi}{\partial t})$ terms are computed in the same manner as they are for (3), the vertical acceleration term in the latitudinal momentum equation.

c. Term three

$$-\frac{\bar{\pi}uu\tan\theta}{a} \equiv \frac{(u\bar{\pi}u)_{ijk}\tan\theta_j}{a} \tag{20}$$

where $\bar{\pi}$ is computed as in (1.1).

d. Term four

$$\pi uf = f_j(\bar{\pi}u)_{ijk} \tag{21}$$

where $\bar{\pi}$ is obtained as in (1.1).

e. Term five

$$-\frac{1}{a}[RT\frac{\partial\pi}{\partial\theta} + \pi\frac{\partial\phi}{\partial\theta}] \equiv$$

$$-\frac{1}{a}[R\bar{T}_{ijk}(\frac{\partial\pi}{\partial\theta})^*_{ij} + \bar{\pi}_{ij}\frac{(\phi_{L,j+1,k} - \phi_{L,j-1,k})}{2\Delta\theta}] \tag{22}$$

where $L = i$ (j even)

$L = i-1$ (j odd)

$\bar{\pi}$ is obtained from (1.1) and $\bar{T}$ is computed in a similar manner. The computation of $(\frac{\partial\pi}{\partial\theta})^*$ is carried out in the same manner as the computation of $(\frac{\partial\pi}{\partial\lambda})^*$ for Equation (10) with the exception that the $(\frac{\partial\pi}{\partial\theta})^*$ in this case is computed along a meridian instead of a latitude circle. Refer to Equations (10), (11), (12), (13), (14), (15), and (16).

Thermodynamic equation

1. Left hand side

$$\frac{\partial(\pi T)}{\partial t} \equiv \frac{(\pi T)^{n+1}_{ijk} - (\pi T)^{n-1}_{ijk}}{2\Delta t} \tag{23}$$

This term is computed directly at the poles.

2. Right hand side

a. Term one

$$-\frac{1}{a\cos\theta}[\frac{\partial(\pi uT)}{\partial\lambda} + \frac{\partial(\pi vT\cos\theta)}{\partial\theta}] \equiv -\frac{1}{a\cos\theta_j}[\frac{(\bar{T}u\bar{\pi})_{i+1,j,k} - (\bar{T}u\bar{\pi})_{ijk}}{2\Delta\lambda}$$

$$+\frac{(Tv\bar{\pi})_{L,j+1,k}\cos\theta_{j+1} - (\bar{T}v\bar{\pi})_{L,j-1,k}\cos\theta_{j-1}}{2\Delta\theta}] \tag{24}$$

where

$$L = i \quad (j \text{ odd})$$

$$L = i+1 \quad (j \text{ even})$$

$\bar{\pi}$ is computed as in (1.1) and $\bar{T}$ is computed in a similar manner. At 85°S $(\bar{T}v\bar{\pi})_{L,j-1,k}$ is undefined and not included in the difference equation. At 85°N $(\bar{T}v\bar{\pi})_{L,j+1,k}$ is undefined and not included. The computation of (24) at the poles is carried out as discussed in Section II-D-2 (Polar Finite Differencing). At the north pole the expression used for term one, (24), is

$$\text{R.H.S. term 1} \equiv -\frac{2}{a\Delta\theta 36}\sum_{i=1}^{36}(\bar{T}v\bar{\pi})_{i,35,k} \tag{25}$$

In order to compute this term at the south pole change the sign of $(\bar{T}v\bar{\pi})$ and the subscript j to 1.

b. Term two

$$\pi\frac{\partial(wT)}{\partial\sigma} = \pi_{ij}\left[\frac{w_{ijk}(T_{i,j,k+1}+T_{ijk})-w_{i,j,k-1}(T_{ijk}+T_{i,j,k-1})}{2\Delta\sigma}\right] \tag{26}$$

where Equations (4) and (5) are used to compute w. This term is computed directly at the poles.

c. Term three

$$\frac{RT}{C_p\sigma}\left[-w\pi+\sigma\left(\frac{\partial\pi}{\partial t}+\frac{1}{a\cos\theta}\left[u\left(\frac{\partial\pi}{\partial\lambda}\right)+v\left(\frac{\partial\pi}{\partial\theta}\right)\cos\theta\right]\right)\right] \equiv$$

$$\frac{RT_{ijk}}{C_p\sigma_k}\left[-\frac{(w_{ijk}+w_{i,j,k-1})\pi_{ij}}{2}+\sigma_k\left(\left(\frac{\partial\pi}{\partial t}\right)_{ij}\right.\right.$$

$$+\frac{1}{a\cos\theta_j}\left[\frac{(u\bar{\pi})_{i+1,j,k}-(u\bar{\pi})_{ijk}}{2\Delta\lambda}-\frac{\pi_{ij}(u_{i+1,j,k}-u_{ijk})}{2\Delta\lambda}\right.$$

$$\left.\left.+\cos\theta_j\frac{((v\bar{\pi})_{L,j+1,k}-(v\bar{\pi})_{L,j-1,k})}{2\Delta\theta}-\cos\theta_j\pi_{ij}\frac{(v_{L,j+1,k}-v_{L,j-1,k})}{2\Delta\theta}\right]\right)\Bigg] \tag{27}$$

where

$$L = i \quad (j \text{ odd})$$

$$L = i+1 \quad (j \text{ even}).$$

w is computed by (4), $(\frac{\partial \pi}{\partial t})$ by (5), and π by (1.1). Note a special scheme is used to compute the derivatives of terrain pressure in this equation in order to reduce truncation error. At 85°S $- \bar{v\pi}_{L,j-1,k}$ and $- v_{L,j-1,k}$ are undefined and not included in the difference equation. At 85°N $\bar{v\pi}_{L,j+1,j}$ and $v_{L,j+1,k}$ are undefined and not included. The computation of (27) at the poles is carried out as discussed in Section II-D-2 (Polar Finite Differencing). At the north pole the expression used for term three (27) is

$$\text{R.H.S. term 3} \equiv \frac{RT_{pole,k}}{C_p \sigma_k}\left[-\frac{(w_{pole,k} + w_{pole,k-1})\pi_{pole}}{2} + \sigma_k\left(\frac{\partial \pi}{\partial t}_{pole} + \frac{2}{a\Delta\theta 36}\sum_{i=1}^{36}\left[(\bar{v\pi})_{i,35,k} - \pi_{i,35}v_{i,35,k}\right]\right)\right] \qquad (28)$$

In order to compute this term at the south pole change the sign of $(\bar{v\pi})$ and (πv) and change the subscript j to 1.

Moisture equation

1. Left hand side

$$\frac{\partial q\pi}{\partial t} \equiv \frac{(q\pi)^{n+1}_{ijk} - (q\pi)^{n-1}_{ijk}}{2\Delta t} \qquad (29)$$

This term is computed directly at the poles.

2. Right hand side

   a. Term one

$$- \frac{1}{a \cos \theta} \left[\frac{\partial(u\pi q)}{\partial \lambda} + \frac{\partial(v\pi q \cos \theta}{\partial \theta}\right] \equiv - \frac{1}{a \cos\theta_j}\left[\frac{(\bar{q}\bar{u}\bar{\pi})_{i+1,j,k} - (\bar{q}\bar{u}\bar{\pi})_{ijk}}{2\Delta\lambda}\right.$$

$$\left. + \frac{(\bar{q}\bar{v}\bar{\pi})_{L,j+1,k}\cos\theta_{j+1} - (\bar{q}\bar{v}\bar{\pi})_{L,j-1,k}\cos\theta_{j-1}}{2\Delta\theta}\right] \qquad (30)$$

where

$$L = i \quad (j \text{ odd})$$

$$L = i+1 \quad (j \text{ even})$$

$\bar{\pi}$ is computed as in (1.1) and $\bar{q}$ is computed in a similar manner. At 85°S $(\bar{q}\bar{v}\bar{\pi})_{L,j-1,k}$ is undefined and at 85°N $(\bar{q}\bar{v}\bar{\pi})_{L,j+1,k}$ is undefined. Undefined terms are not included in the difference equations. The computation of (30) at the poles is as discussed in Section II-D-2 (Polar Finite Differencing). At the north pole the expression used for term one, (30), is

$$\text{R.H.S. term 1} \equiv - \frac{2}{a\Delta\theta 36} \sum_{i=1}^{36} (\bar{q}\bar{v}\bar{\pi})_{i,35,k} \qquad (31)$$

In order to compute this term at the south pole reverse the sign of $(\bar{q}\bar{v}\bar{\pi})$ and change the subscript j to 1.

b. Term two

$$\pi \frac{\partial(wq)}{\partial\sigma} = \pi_{ij}\left[\frac{w_{ijk}(q_{i,j,k+1}+q_{ijk}) - w_{i,j,k-1}(q_{ijk}+ q_{i,j,k-1})}{2\Delta\sigma}\right] \qquad (32)$$

where Equations (4) and (5) are used to compute w. This term is computed directly at the poles.

Hydrostatic equation

The hydrostatic equation is integrated to form the hypsometric equation

$$\Delta\phi = -R\bar{T}\ \Delta\ \ell n\ \sigma \qquad (33)$$

This is converted to a difference equation which is a modified form of that used by Kesel and Winninghoff (1972).

$$\phi_{i,j,k+1} =$$

$$\phi_{ijk} - R\ell n\left(\frac{\sigma_{k+1}}{\sigma_k}\right)\left[\frac{T_{ijk}(\ell n\sigma_k + \ell n\pi_{ij}) + T_{i,j,k+1}(\ell n\sigma_{k+1} + \ell n\pi_{ij})}{\ell n\sigma_k + \ell n\sigma_{k+1} + 2\ell n\pi_{ij}}\right] \qquad (34)$$

For the lowest layer (34) is modified to form

$$\phi_{ij1} = -RT_{ij1}\,\ell n\sigma_1 \qquad (35)$$

Both (34) and (35) are computed directly at the poles.

APPENDIX B

TERMS USING FOURTH ORDER FINITE DIFFERENCING IN MIXED SECOND AND FOURTH ORDER SCHEME

Williams (1972) has concluded that fourth order differencing used only in the advection terms and the divergence term of the continuity equation will improve the phase speed of meteorological waves while keeping the necessary reduction in the time step to a minimum. The following equations are the advection terms and the divergence term in fourth order finite difference form as developed by Mihok (1974) for use in the global model.

The advection term for the latitudinal momentum equation is

$$-\frac{1}{a\cos\theta_j}\Big[\frac{4}{3}\Big\{\frac{(u_{ijk}+u_{i+1,j,k})\overline{u\bar{\pi}}_{i+1/2,j,k}-(u_{ijk}+u_{i-1,j,k})\overline{u\bar{\pi}}_{i-1/2,j,k}}{2\cdot 2\Delta\lambda}$$

$$+\frac{(u_{ijk}+u_{i,j+2,k})\overline{v\bar{\pi}}_{i,j+1,k}\cos\theta_{j+1}-(u_{ij}+u_{i,j-2,k})\overline{v\bar{\pi}}_{i,j-1,k}\cos\theta_{j-1}}{2\cdot 2\Delta\theta}\Big\}$$

$$-\frac{1}{3}\Big\{\frac{(u_{ijk}+u_{i+2,j,k})\overline{u\bar{\pi}}_{i+1,j,k}-(u_{ijk}+u_{i-2,j,k})\overline{u\bar{\pi}}_{i-1,j,k}}{2\cdot 4\Delta\lambda}$$

$$+\frac{(u_{ijk}+u_{i,j+4,k})\overline{v\bar{\pi}}_{i,j+2,k}\cos\theta_{j+2}-(u_{ijk}+u_{i,j-4,k})\overline{v\bar{\pi}}_{i,j-2,k}\cos\theta_{j-2}}{2\cdot 4\Delta\theta}\Big\}\Big] \qquad (1)$$

where the $\overline{u\bar{\pi}}_{i+1/2,j,k}$, $\overline{u\bar{\pi}}_{i-1/2,j,k}$, $\overline{v\bar{\pi}}_{i,j+1,k}$ and $\overline{v\bar{\pi}}_{i,j-1,k}$ are given by (2.1) and (2.2) in Appendix A. Note that

$$\overline{\overline{u\bar{\pi}}}_{i+1,j,k} \equiv$$

$$\frac{1}{4}[(u\bar{\pi})_{ijk}+(u\bar{\pi})_{i+2,j,k}+(u\bar{\pi})_{i+1,j+2,k}+(u\bar{\pi})_{i+1,j-2,k}] \tag{1.1}$$

$\overline{u\bar{\pi}}_{i-1,j,k}$ is obtained from (1.1) by incremental subscripting.

$$\overline{\overline{v\bar{\pi}}}_{i,j+2,k} =$$

$$\frac{1}{4}[(v\bar{\pi})_{ijk}+(v\bar{\pi})_{i-1,j+2,k}+(v\bar{\pi})_{i+1,j+2,k}+(v\bar{\pi})_{i,j+4,k}] \tag{1.2}$$

and $\overline{\overline{v\bar{\pi}}}_{i,j-2,k}$ is obtained from (1.2) by incremental subscripting.

If one substitutes v everywhere for u in (1), the result is the longitudinal momentum equation.

The advection term for the thermodynamic equation is given by

$$-\frac{1}{a\cos\theta_j}\left[\frac{4}{3}\left\{\frac{(\bar{T}u\bar{\pi})_{i+1,j,k}-(\bar{T}u\bar{\pi})_{ijk}}{2\Delta\lambda}\right.\right.$$

$$\left.+\frac{(\bar{T}v\bar{\pi})_{i,j+1,k}\cos\theta_{j+1}-(\bar{T}u\bar{\pi})_{i,j-1,k}\cos\theta_{j-1}}{2\Delta\theta}\right\}$$

$$-\frac{1}{3}\left\{\frac{(\bar{T}^*[u\bar{\pi}]^*)_{i+1,j,k}-(\bar{T}^*[u\bar{\pi}]^*)_{i-1,j,k}}{4\Delta\lambda}\right.$$

$$\left.\left.+\frac{(\bar{T}^*[v\bar{\pi}]^*)_{i,j+2,k}\cos\theta_{j+2}-(\bar{T}^*[v\bar{\pi}]^*)_{i,j-2,k}\cos\theta_{j-2}}{4\Delta\theta}\right\}\right] \tag{2}$$

where $\bar{\pi}$ is computed as in (1.1) of Appendix A and $\bar{T}$ is computed in a similar manner. Note that

$$\bar{T}^*_{i+1,j,k} = \frac{1}{4}[\bar{T}_{L,j,k} + \bar{T}_{L,j+1,k} + \bar{T}_{M,j,k} + \bar{T}_{L,j-1,k}] \tag{2.1}$$

$$\bar{T}^*_{i-1,j,k} = \frac{1}{4}[\bar{T}_{N,j,k} + \bar{T}_{N,j+1,k} + \bar{T}_{O,j,k} + \bar{T}_{N,j,k}] \tag{2.2}$$

$$\bar{T}^*_{i,j+2,k} = \frac{1}{4}[\bar{T}_{L,j+2,k} + \bar{T}_{L,j+3,k} + \bar{T}_{M,j+2,k} + \bar{T}_{L,j+1,k}] \tag{2.3}$$

and $\bar{T}^*_{i,j-2,k}$ is obtained from (2.3) by incremental subscripting.

In the above equations

L = i+1 (j odd)

L = i+2 (j even)

M = i+2 (j odd)

M = i+2 (j even)

N = i-1 (j odd)

N = i (j even)

O = i (j odd)

O = i-1 (j even)

The expressions for $[u\bar{\pi}]^*$ can be obtained by substituting $u\bar{\pi}$ in for $\bar{T}$ in the above equations.

Quantities with a bar, e.g. $\bar{T}$, are applicable at velocity points while starred quantities, e.g. $\bar{T}^*$, are applicable at mass points. The advection term for the moisture equation is the same as (2) with q substituted for T .

The divergence term of the continuity equation is

$$\frac{1}{a\cos\theta_j}\left[\frac{4}{3}\left\{\frac{(u\bar{\pi})_{i+1,j,k}-(u\bar{\pi})_{ijk}}{2\Delta\lambda}+\frac{(v\bar{\pi})_{i,j+1,k}\cos\theta_{j+1}-(v\bar{\pi})_{i,j-1,k}\cos\theta_{j-1}}{2\Delta\theta}\right\}\right.$$

$$\left.-\frac{1}{3}\left\{\frac{[u\bar{\pi}]^*_{i+1,j,k}-[u\bar{\pi}]^*_{i-1,j,k}}{4\Delta\lambda}+\frac{[v\bar{\pi}]^*_{i,j+2,k}\cos\theta_{j+2}-[v\bar{\pi}]^*_{i,j-2,k}\cos\theta_{j-2}}{4\Delta\theta}\right\}\right] \qquad (3)$$

where $\bar{\pi}$ is given by (1.1) in Appendix A and the $[u\bar{\pi}]^*$ quantities are computed as in the thermodynamic equation.

Mihok (1974) blended the mixed second and fourth order scheme with the normal second order scheme at 75° latitude. This was done to avoid differencing over the poles.

LIST OF REFERENCES

1. Arakawa, A., "Computational Design for Long-Term Numerical Integration of the Equations of Fluid Motion: Two Dimensional Incompressible Flow. Part I." Journal of Computational Physics, 1, No. 1, Academic Press, Inc., New York, 119-143, 1966.

2. _____, Katayama, Akira, and Mintz, "Numerical Simulation of the General Circulation of the Atmosphere." Proceedings of the WMO/IUGG Symposium on Numerical Weather Prediction, Tokyo, Japan, November 26 - December 4, 1968, Japan Meteorological Agency, Tokyo, IV-1 - IV-14, 1969.

3. _____, and Mintz, "The UCLA General Circulation Model," Department of Meteorology, University of California, Los Angeles, Workshop Notes, 25 March - 4 April 1974, VI-1 - VI-8, VII-3 - VII-7, 1974.

4. Elias, T. E., Numerical Experiments with a Five-Level Global Atmospheric Prediction Model Using a Staggered, Spherical, Sigma Coordinate System, M. S. Thesis, Naval Postgraduate School, Monterey, California, 1973.

5. Gates, W. L., and Reigel, C. A., "A Study of Numerical Errors in the Integration of Barotropic Flow on a Spherical Grid." J. of Geophy. Res., 67, No. 2, 773-784, 1962.

6. Haltiner, G. J., Numerical Weather Prediction, 1-39, 90-114, 193-196, 220-243, Wiley, 1971.

7. _____, and Martin, F. L., Dynamical and Physical Meteorology, 52-53, McGraw-Hill, 1957.

8. _____, and Williams, R. T., Numerical Weather Prediction: Some Problems and Solutions, Problem Set, Naval Postgraduate School, Monterey, California, 1973.

9. Haurwitz, B., "The Motion of Atmospheric Disturbances on the Spherical Earth." J. Marine Research (Sears Foundation), 3, 254-267, 1940.

10. Heburn, G. W., Numerical Experiments with Several Time Differencing Schemes with a Barotropic Primitive Equation Model on a Spherical Grid, M. S. Thesis, Naval Postgraduate School, Monterey, California, 1972.

11. Holloway, J. L., Spelman, M. J., and Manabe, S., "Latitude-Longitude Grid Suitable for Numerical Time Integration of a Global Atmospheric Model." Mon. Wea. Rev., 101, No. 1, 69-78, 19 .

12. Jeffreys and Jeffreys, Methods of Mathematical Physics, Cambridge, 429-431, 1956.

13. Kesel and Winninghoff, "The Fleet Numerical Weather Central Operational Primitive-Equation Model." Mon. Wea. Rev., 100, No. 5, 360-373, 1972.

14. Kurihara, Y., "Note on Finite Difference Expressions for the Hydrostatic Relation and Pressure Gradient Force." Mon. Wea. Rev., 96, No. 9, 654-656, 19 .

15. Mihok, W. F., Fourth-Order Differencing in a Five-Layer Spherical Sigma Coordinate Global Weather Prediction Model, M. S. Thesis, Naval Postgraduate School, Monterey, California, 1974.

16. McCollough, J. M., Initialization of a 5-Level Global Atmospheric Circulation Model Using a Staggered, Spherical, Sigma Coordinate System, M. S. Thesis, Naval Postgraduate School, Monterey, Calif., 1974.

17. Neamtan, S. M., "The Motion of Harmonic Waves in the Atmosphere." J. Meteorology, 3, 53-56, 1946.

18. Phillips, N. A., "Numerical Integration of the Primitive Equations on the Hemisphere." Mon. Wea. Rev., 333-345, 1959.

19. Robert, Andre, "The Behavior of Planetary Waves in an Atmospheric Model Based on Spherical Harmonics," Publication in Meteorology No. 77, Clearinghouse for Federal Scientific and Technical Information (CFSTI), Springfield, Virginia, 56-62, 1965.

20. Smagorinsky et al, "Numerical Results from a Nine-Level General Circulation Model of the Atmosphere." Mon. Wea. Rev., 93, No. 12, 727-768, 1965.

21. Williams, R. T., "Phase Speed Errors with Second and Fourth Order Space Differences with Staggered and Unstaggered Grids," Naval Postgraduate School Report NPS-51Wu72031A, March 1972.

INITIAL DISTRIBUTION LIST

		No. Copies
1.	Defense Documentation Center Cameron Station Alexandria, Virginia 22314	2
2.	Library, Code 0212 Naval Postgraduate School Monterey, California 93940	2
3.	Dr. George J. Haltiner (Code 51Ha), Chairman Department of Meteorology Naval Postgraduate School Monterey, California 93940	5
4.	Dr. Roger T. Williams, Code 51Wu Department of Meteorology Naval Postgraduate School Monterey, California 93940	5
5.	Lieutenant William T. Elias U. S. Fleet Weather Central Box 31 FPO New York 09540	1
6.	Officer in Charge Environmental Prediction Research Facility Naval Postgraduate School Monterey, California 93940	2
7.	Commanding Officer Fleet Numerical Weather Central Naval Postgraduate School Monterey, California 93940	2
8.	LCDR Wayne R. Lambertson USN Fleet Numerical Weather Central Naval Postgraduate School Monterey, California 93940	1
9.	ARCRL - Research Library Attn: Nancy Davis/Stop 29 L. G. Hanscom Field Bedford, Massachusetts 01730	1

10. Director, Naval Research Laboratory — 1
Attn: Tech. Services Info. Officer
Washington, D. C. 20390

11. American Meteorological Society — 1
45 Beacon Street
Boston, Massachusetts 02128

12. Department of Meteorology, Code 51 — 3
Naval Postgraduate School
Monterey, California 93940

13. Department of Oceanography, Code 58 — 1
Naval Postgraduate School
Monterey, California 93940

14. Office of Naval Research — 1
Department of the Navy
Washington, D. C. 20360

15. Commander, Air Weather Service — 2
Military Airlift Command
U. S. Air Force
Scott Air Force Base, Illinois 62226

16. Atmospheric Sciences Library — 1
National Oceanic and Atmospheric Administration
Silver Spring, Maryland 20910

17. National Center for Atmospheric Research — 1
Box 1470
Boulder, Colorado 80302

18. Dr. T. N. Krishnamurti — 1
Department of Meteorology
Florida State University
Tallahassee, Florida 32306

19. Dr. Fred Shuman, Director — 1
National Meteorological Center
World Weather Building
Washington, D. C. 20233

20. Dr. J. Smagorinsky, Director — 1
Geophysical Fluid Dynamics Laboratory
Princeton University
Princeton, New Jersey 08540

21. Dr. A. Arakawa — 1
Department of Meteorology
University of California
Los Angeles, California 90024

22. Professor N. A. Phillips, 54-1422 — 1
National Meteorological Center
National Oceanic and Atmospheric Administration
World Weather Building
Washington, D. C. 20233

23. Dr. Russell Elsberry, Code 51Es — 1
Department of Meteorology
Naval Postgraduate School
Monterey, California 93940

24. Dr. Jerry D. Mahlman — 1
Geophysical Fluid Dynamics Laboratory
Princeton University
Princeton, New Jersey 08540

25. Dr. Robert L. Haney, Code 51Hy — 1
Department of Meteorology
Naval Postgraduate School
Monterey, California 93940

26. Dr. Ron L. Alberty — 1
National Severe Storms Laboratory
University of Oklahoma
Norman, Oklahoma 73069

27. Dr. W. L. Gates — 1
The RAND Corporation
1700 Main Street
Santa Monica, California 90406

28. Dr. Richard Alexander — 1
The RAND Corporation
1700 Main Street
Santa Monica, California 90406

29. Commanding Officer — 1
Fleet Weather Central
Box 110
FPO San Francisco 96610

30. Dr. F. J. Winninghoff — 1
1085 Steeles Avenue #503
Willowdale (Toronto), Ontario M2R2%1

31. LCDR P. G. Kesel, ODSI — 1
2460 Garden Road
Monterey, California 93940

32. Mr. Leo C. Clarke — 1
Fleet Numerical Weather Central
Naval Postgraduate School
Monterey, California 93940

33. Naval Weather Service Command — 1
Washington Navy Yard
Washington, D. C. 20374

34. Naval Oceanographic Office — 1
Library (Code 3330)
Washington, D. C. 20373

35. Lieutenant William F. Mihok — 1
Fleet Numerical Weather Central
Naval Postgraduate School
Monterey, California 93940

36. Lieutenant Dennis E. Maher — 2
USS HALEAKALA AE-25
FPO San Francisco 96601

37. Mr. Richard Perry — 1
Environmental Prediction Research Facility
Naval Postgraduate School
Monterey, California 93940

38. Dr. S. Piacsek — 1
Code 7750
Naval Research Laboratory
Washington, D. C. 20375

Thesis
M27715 Maher
c.1 155236

Experiments with a 5-level global primitive equation atmospheric model using analytically determined fields.